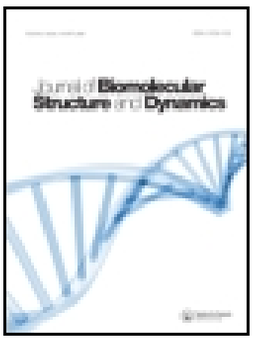

Journal of Biomolecular Structure and Dynamics

ISSN: 0739-1102 (Print) 1538-0254 (Online) Journal homepage: https://www.tandfonline.com/loi/tbsd20

2D and 3D QSAR modelling, molecular docking and *in-vitro* evaluation studies on 18β-glycyrrhetinic acid derivatives against triple negative breast cancer cell line

Aparna Shukla, Rekha Tyagi, Sanjeev Meena, Dipak Datta, Santosh Kumar Srivastava & Feroz Khan

To cite this article: Aparna Shukla, Rekha Tyagi, Sanjeev Meena, Dipak Datta, Santosh Kumar Srivastava & Feroz Khan (2019): 2D and 3D QSAR modelling, molecular docking and *in-vitro* evaluation studies on 18β-glycyrrhetinic acid derivatives against triple negative breast cancer cell line, Journal of Biomolecular Structure and Dynamics, DOI: 10.1080/07391102.2019.1570868

To link to this article: https://doi.org/10.1080/07391102.2019.1570868

Accepted author version posted online: 28 Jan 2019.

2D and 3D QSAR modelling, molecular docking and *in-vitro* evaluation studies on 18β-glycyrrhetinic acid derivatives against triple negative breast cancer cell line

Aparna Shukla[1], Rekha Tyagi[2], Sanjeev Meena[3], Dipak Datta[3], Santosh Kumar Srivastava[2], Feroz Khan[1,*]

[1]Metabolic and Structural Biology Department, CSIR-Central Institute of Medicinal and Aromatic Plants, P.O.-CIMAP, Kukrail Picnic Spot Road, Lucknow, 226015, UP, India

[2]Medicinal Chemistry Division, Central Institute of Medicinal and Aromatic Plants, P.O. CIMAP, Lucknow 226015, India

[3]Biochemistry Division, CSIR-Central Drug Research Institute (CDRI), Lucknow, 226031, India,

***Corresponding Author:**

Dr. Feroz Khan

Metabolic & Structural Biology Department,

Plant Biology Division,

CSIR-Central Institute of Medicinal and Aromatic Plants

P.O. CIMAP, Kukrail Picnic Spot Road,

Lucknow-226015 (Uttar Pradesh), INDIA

Phone: +91 522 2718668 (Lab); +91 522 2342666 (Fax)

Email: f.khan@cimap.res.in

Abstract

Triple negative breast cancers (TNBC) are one of the most aggressive and complex forms of cancers in women. TNBCs are commonly known for their complex heterogeneity and poor prognosis. The present work aimed to develop a predictive 2D and 3D quantitative structure activity relationship (QSAR) models against metastatic TNBC cell line. The 2D-QSAR was based on multiple linear regression analysis and validated by Leave-One-Out (LOO) and external test set prediction approach. QSAR model presented regression coefficient values for training set (r^2), LOO based internal regression (q^2) and external test set regression (pred_r^2) are 0.84, 0.82 and 0.75 respectively. Five properties, Epsilon4 (electronegativity), ChiV3cluster (valence molecular connectivity index), chi3chain (retention index for three membered ring), TNN5 (nitrogen atoms separated through 5 bond distance) and nitrogen counts were identified as important structural features responsible for anticancer activity of MDA-MB-231 inhibitors. Five novel derivatives of Glycyrrhetinic acid (GA) named GA-1, GA-2, GA-3, GA-4 and GA-5 were semi-synthesised and screened through the QSAR model. Further, *in-vitro* activities of the derivatives were analysed against human TNBC cell line, MDA-MB-231. The result showed GA-1 exhibit improved cytotoxic activity to that of parent compound (GA). Further, Atomic Property Field (APF) based 3D QSAR and scoring recognise C-30 carboxylic group of GA-1 as major influential factor for its anticancer activity. The significance of C-30 carboxylic group in GA derivatives were also confirmed by molecular docking study against cancer target Glyoxalase-I. Finally, the oral bioavailability and toxicity of GA-1 was assessed by computational ADMET studies.

Keywords: QSAR, Breast cancer, Triple négative breast cancer, Glycyrrhetinic acid, MDA-MB-231, Glyoxalase-I

Introduction

Breast cancer is most frequently diagnosed cancer and second leading cause of female deaths worldwide. In majority of cases mortality is due to its metastatic dissemination to distant sites (Polyak, *et al.*, 2011). Despite the enormous medical importance of metastasis, its molecular underpinning remains insufficiently understood because of its intertumor and intratumor heterogeneity (Ovcaricek, *et al.*, 2011 & Bianchini, *et al.*, 2016). Breast carcinomas, demarcated as triple negative breast cancers (TNBC), are highly aggressive and do not express progesterone receptor (PR), estrogen receptor (ER), and human epidermal growth factor receptor2 (HER2) (Thike, *et al.*, 2010). Consequently, it is resistant to hormone targeted therapies and only 20% of TNBC respond well to standard chemotherapy using anthracycline-based (doxorubicin plus cyclophosphamide) or paclitaxel chemotherapy etc. (Zardavas, *et al.*, 2013). Thus, in current breast cancer research, developing improved treatment for metastatic TNBC is one of the highest priorities. Several researches have been carried out to understand metastatic TNBC cells sensitivity towards plant based different chemical scaffolds (Iqbal, *et al.*, 2018). Recent prognosis work on TNBC focusing on targets PARP1, mTOR, TGF-β from Notch signalling, Wnt/β-catenin and Hedgehog pathways (Jamdade, *et al.*, 2015; Wein, *et al.*, 2018 & Badve, *et al*., 2011).

Glycyrrhiza glabra, an Indian medicinal herb, also known as licorice, contains biologically active triterpenoid glycyrrhizic acid. Glycyrrhizic acid is a diglucopyranosiduronic acid of the glycyrrhetinic acid (GA) (Tewari, *et al.*, 2017). Substantial research has been carried out on human liver metabolism of Glycyrrhizic acid. Reto Karpf in year 1994 revealed Glycyrrhizic acid transformed into its aglycone form GA through intestinal bacteria when orally administered (Krähenbühl, *et al.*, 1994). In cancer research GA is mostly explored for its activity against human hepatocellular carcinoma (HCC) cells since an earlier work revealed the existence of GA receptor on rat and human hepatocytes surface (Negishi, *et al.*, 1991). It has been reported that anti-HCC response of GA is mediated through inhibition of immune response by regulating T cells, cell cycle arrest, induction of cell apoptosis and autophagy (Cai, *et al.*, 2017). Evidently, GA has been identified to exhibit remarkable anticancer activities. Therefore, over the past decade, GA has been serving as a good structural template for more potent anticancer agents. Many groups have studied the effects of structural modification in GA on the cytotoxicity of various human cancer cell lines (Xu, *et al.*, 2017). Despite these capabilities, the mechanisms of action of GA in metastatic TNBC has not been investigated so far.

Notably, our earlier work on GA and its novel derivatives against breast cancer MCF-7 displayed good anticancer potency (Yadav, *et al.*, 2014, Yadav, *et al*., 2013). Therefore, the present work was designed to combat metastatic TNBC cell lines using biological effects of GA and its novel derivatives. The work includes chemical feature identification of metastatic TNBC cell inhibitors through regression based quantitative structure activity relationship (QSAR) model (Yadav, *et al.*, 2013). Further, five novel GA derivatives were semi-synthesised and screened through the prepared QSAR model. The derivatives were further investigated for *in-vitro* activity in metastatic breast cancer cell line MDA-MB-231. Subsequently, atomic property field (APF) based 3D QSAR model was generated to explore atomic property field (APF) and structure activity relationship of synthesised derivatives. The

anticancer mechanism of action of GA derivatives on TNBC drug targets were explored through molecular docking studies. In TNBC cells enzyme Glyoxalase-I (GLO-I) inhibition leads to increased level of alpha-oxoaldehydes that cause increase in apoptosis, supress migration and invasion of metastatic breast cancer. Therefore, GLO-I is considered as one of the promising TNBC target. Here, molecular docking and 3D-QSAR modelling was performed considering Glyoxalase-I as a promising TNBC drug target. The oral bioavailability and possible toxicity were also assessed through computational ADMET (absorption, distribution, metabolism, excretion and toxicity) analysis.

Materials and Method

Computational 2D QSAR modelling for GA derivative designing

Dataset collection and structure preparation

The modelling set comprising 144 compounds, metastatic TNBC cell line, MDA-MB-231 inhibitors (Table S1; training set and Table S2; test set compounds, Supplementary materials) collected from the ChEMBL database and reported literatures (Goldbrunner, *et al.,* 1997; Gao, *et al.,* 2014; He, *et al.,* 2015; Yang, *et al.,* 2016 & Motiwala, *et al.,* 2013). The modelling set exhibits plant-product inspired scaffolds, comprises with 2-5 fused rings skeleton (Table S3, Supplementary materials).

The structural drawing and geometry cleaning of the modelling set compounds were performed through, ChemBioOffice suite Ultra v12.0 (2015) software (CambridgeSoft Corp., UK). Further, each compound subjected to energy minimization to get optimized bond distance, bond angles and set dihedrals by applying MMFF force field. Moreover, the method adds additional properties to the compounds including initial potential energy, RMS gradient, MMFF energy and minimization criteria.

Chemical descriptors calculation

For QSAR model generation, the compounds were denoted by structural descriptors or physico-chemical properties. Computation for descriptors were done by using VLife MDS v4.4 (2014) software (VLife Technologies, NovaLead Pharma Pvt. Ltd. India). Software Vlife, calculate structural descriptors, belonging to major classes *viz.,* (a) physicochemical descriptors, (b) extended topochemical descriptors and (c) alignment independent descriptors.

QSAR model generation

Primarily, the dataset of 144 compounds was divided into 70% as training set and 30% as external test set applying random selection technique using Vlife. The PIC_{50} (μM) value was assigned as dependent variable. PIC_{50} is a negative logarithm of IC_{50} value, expressed in molar concentration. The physicochemical properties or structural descriptors were considered as independent variables. Invariable descriptors with zero or equal values were deleted. The regression coefficient for training set (100 compounds) was calculated by using equation 1. Where, yi and $\hat{y}_i$ signify the actual and predicted PIC_{50} of i^{th} compound respectively. Whereas y_{mean} is the average/mean value of actual PIC_{50} of training set compounds.

$$r^2 = \frac{\sum(y_i - \hat{y}_i)^2}{\sum(y_i - y_{mean})^2}$$

(Equation 1)

QSAR model generation criteria and parameter used for feature selection

The 2D QSAR model was developed by applying multiple linear regression (MLR) approach. A stepwise forward-backward selection criterion was applied for feature/descriptor extraction. Continuous multiple variable based MLR model was generated, step by step depending on Fischer coefficient values (F values). The F test gives the statistical significance of the descriptor. The F_{test} in and F_{test} out values were set at 4 and 3. The predictor descriptors were identified by these stepping criteria. The search is terminated when addition of additional variables is no longer needed. Before model development, inter-correlated descriptors (Correlation >0.70) were discarded.

2D QSAR model validation

To scrutinise the predictability of developed model, leave-one-out (q^2, LOO), external set predictions (r^2_{pred}) and r^2_m matrix were calculated (Cramer III, *et al.*, 1988; Golbraikh, *et al.*, 2002 & Ojha, *et al.*, 2011). A LOO based cross-validated regression coefficient (q^2) was calculated based on equation 2 (Shen *et al.*, 2002). Where yi and $\hat{y}_i$ signify the actual and predicted PIC_{50} value for i^{th} compound. Whereas y_{mean} is the average/mean value of actual PIC_{50} of training set compounds.

$$q^2 = 1 - \frac{\sum(y_i - \hat{y}_i)^2}{\sum(y_i - y_{mean})^2}$$

(**Equation 2**)

The regression for external test set (r^2_{pred}) was calculated by using equation 3 (Kier, *et al.*, 1977& Golbraikh, *et al.*, 2002). r^2_{pred} validate the model predictability for external compounds and verify the model predicted result's reliability.

$$r^2_{pred} = 1 - \frac{\sum\left(y_{i(test)} - \hat{y}_{i(test)}\right)^2}{\sum\left(y_{i(test)} - y_{mean(test)}\right)^2}$$

(**Equation 3**)

Randomization test

The robustness of generated model was also assessed by calculating Z score values using equation 4. Where h, μ and σ signifies r^2 of original dataset, average values of r^2s for random datasets and standard deviation for random dataset. The calculated Z score should be higher

than the tabulated value Zc as reported by Zheng *et al.*, (2000). The higher Z score indicate the null hypothesis is rejected and the model generated from actual dataset is statistically significant.

$$Z = (h - \mu)/\sigma$$ **(Equation 4)**

r^2m matrix for QSAR model validation

The external predictability of developed model was also checked by using r_m^2 matrix method calculating r_0^2, $r_0'^2$, r_m^2, $r_m'^2$, $\overline{r_m^2}$ and r_m^2 (Ojha, *et al.*, 2011). The r_m^2 matrix is measured by using r^2 and r_0^2. Where, r^2 and r_0^2 signify correlation between observed and predicted values with and without intercept for the regression line. Statistical parameters r_0^2, $r_0'^2$, r_m^2, $r_m'^2$, $\overline{r_m^2}$ were computed as mentioned by Roy, *et al.*, 2018. The equation used for r_m^2 parameter calculation is given in equation 5.

$$r_m^2 = r^2\left(1 - \left|\sqrt{r_0^2 - r^2}\right|\right)$$ **(Equation 5)**

Applicability domain (AD) assessment of 2D-QSAR model

A statistically validated model predicted results are considered to be reliable only when the query set compound falls within its applicability domain (AD). Here, three most important criteria were adopted to check the AD of developed model *viz.*, (i) the biological space cover of whole dataset, (ii) the chemical space cover by training set and test set, (iii) distance-based distribution of training and test set in structure and activity space (Jaworska, *et al.*, 2005). A 3D principal component analysis (PCA) was applied to compute projection of chemical space of test set within training set (Adhikari, *et al.*, 2017 & Amin, *et al.*, 2018). A structure similarity based hierarchical cluster analysis was done to assess structure relatedness of training, test and query set compounds (Figure S1, Supplementary material).

Atomic property field (APF) based 3D-QSAR modelling study

An APF based 3D-QSAR was also performed on congeneric series of 42 GA derivatives. An APF based 3D-QSAR thoroughly describe, the spatial arrangement of structural features that bestow specific activity to the molecule. Since, a 3D-QSAR model reliability is highly depend upon the structural filed alignment. Therefore, for 3D-QSAR studies a congeneric series of 42 GA derivatives were taken instead of using total 144 compounds so as to get more homogenous structure space.

A series of 42 GA derivatives with known inhibition activity against MDA-MB-231 were collected from 2D QSAR dataset and reported literatures (Yang, *et al.*, 2016, Yadav, et al., 2014 & Gao, *et al.*, 2014). Their structures were drawn and converted to 3D ICM object using ICM-Chemist v3.8-6a 2018, (Molsoft L.L.C, San Diego, USA) software (Abagyan 2018, http://www.molsoft.com/icm-chemist-pro.html, Totrov, 2008, 2011). The set of 42 GA derivatives were randomly split into 37 training and 5 test set using DS v3.5. The crystal structure of enzyme Glyoxalase-I (GLO-I) bound with GA (2.3 resolution) was retrieved from protein database (PDB: 4PV5). The GLO-I bound conformation of GA was taken as rigid templet structure to which training set structures were aligned based on their APF

energy fields. The APF fields of co-crystallised GA is depicted in figure S5 under supplementary materials. Afterward, for each molecule a 3D based continuous atomic potentials were generated and approximated based on regular space grid. These, continuous potentials represent seven physicochemical properties *viz*., hydrogen bond donor (blue blob) and acceptors (red blob), sp^2 hybridised carbon atoms, molecules lipophilicity (yellow blobs), charge, molecule size and electronegativity or positivity.

Therefore, the training set of 37 compounds can be represented by 259 descriptors. The training and test set molecules were aligned on generated APF fields of co-crystallised GA. For quantitative prediction of novel compound, a partial least square (PLS) based optimal weight distribution was assigned to each molecule based on their APF components. The optimal number of latent vectors for PLS was established by LOO cross-validation on the training set. Then the weighted contributions of each APF components were added together. For external validation randomly selected five compounds were assigned predicted binding values by calculating their fit within the combined QSAR-APF score. The model further utilised to design and screen novel GA derivatives GA-1, GA-2, GA-3, GA-4 and GA-5 based on their APF alignment.

Chemistry

Extraction and chemical synthesis

Five novel 18β-glycyrrhetinic acid derivatives were designed and synthesised modifying C-3 and C-30 positions. Figure 4a represents compound preparation scheme-1 *i.e*., Synthesis of 3-*O*-acyl derivatives of GA and 5b). Figure 4b compound preparation scheme-2 *i.e*., Synthesis of amide derivatives of 3-*O*-acetyl GA.

Isolation of 3β-Hydroxy-11-oxoolean-12-en-29-oic acid (Glycyrrhetinic acid) from Glycyrrhiza glabra:

Extraction and fractionation of *Glycyrrhiza glabra* roots

The roots of *Glycyrrhiza glabra* were air dried under shade and then powdered. This powdered material (2.04 Kg) was extracted with methanol (4 X 5L) at room temperature. The combined methanol extract was subjected for complete solvent removal at 40^{o}C under vacuum. This dried methanolic extract was dissolved in distilled water (2L) and successively extracted with dichloromethane, ethyl acetate and *n*-butanol (4 x 400 ml). The combined dichloromethane, ethyl acetate and *n*-butanol extracts were separately subjected under vacuum distillation at 40^{o}C to yield dichloromethane (99.0g), ethyl acetate (100.0g) extracts and *n*-butanol (56.0g) as given in Figure 1.

Isolation of Glycyrrhizic acid from *n*-BuOH Extract of *Glycyrrhiza glabra* by Flash chromatography

A glass flash column with internal diameter 3 cm and length 23 cm was used. The Flash column was packed with silica gel-H of TLC grade (without binder). The column was tightly packed using vacuum followed by elution of the column with a non-polar solvent (hexane) to make sure nice packing of column. Before loading the extract, glass column was completely

dried and then 1.00 gm of BuOH extract of *Glycyrrhiza glabra* was dissolved in small amount of methanol and with the help of a pipette it was spread onto the glass column without using vacuum, to form a uniform band. The above step was followed by complete drying of the glass column under vacuum. Gradient elution of flash was carried out with a mixture of $CHCl_3$: MeOH in increasing order (up to 50 % MeOH). Fractions of 50ml each were collected. A total of 149 fractions were collected and pooled based on their TLC profile. Excellent separation was achieved due to fine particle size (average size 10 µm) of silica gel-H. The pooled fractions 42-58 (650mg) eluted with $CHCl_3$: MeOH (85:15) was homogeneous and characterized as glycyrrhizic acid (GL) based on its ^{1}H and ^{13}C NMR spectroscopic data (Figure 2).

Acidic hydrolysis of Glycyrrhizic acid (GL) to glycyrrhetinic acid (GA)

Glycyrrhizic acid (650.0 mg obtained from from Flash chromatographic fractions 42-58) was dissolved in 25 ml of 10% H_2SO_4 solution in MeOH and reaction mixture was refluxed for 3-4 hrs, which was further diluted with water and neutralized with 10% NaOH solution and then it was extracted thrice with $CHCl_3$. The combined $CHCl_3$ extract was dried under vacuum, which afforded aglycone (450mg). This aglycone was purified over flash using Silica gel H. A total of 148 fractions were collected and pooled based on their TLC profile. The fractions 29-46 eluted with $CHCl_3$ MeOH (99:1) afforded homogeneous product (GA, 250mg) characterized as glycyrrhetinic acid (GA) on the basis of its ^{1}H and ^{13}C NMR spectroscopic data.18β-glycyrrhetinic acid (Figure 3).

Semi-Synthesis of Glycyrrhetinic Acid (GA) derivatives

The chemical reactions for the synthesis of 3-*O*-acyl derivatives and 3-*O*-acetyl amide derivatives are depicted in schemes-1&2 respectively. All the acyl derivatives were synthesized by taking GA and corresponding acyl chloride (2 equivalent) and a catalytic amount of 4-(N, N-dimethyl) aminopyridine (DMAP) into dry pyridine as solvent and refluxing the reaction mixture for 8 hours up to 80^{o}C (Figure 4a). Reaction mixture was then neutralised with 5% HCl solution and extracted thrice with ethyl acetate. The combined ethyl acetate fraction was washed with water, dried over anhydrous Na_2SO_4 and solvent removed under vacuum to yield the crude product. Further, the crude product was purified by column chromatography which afforded the desired products.

All the 3-*O*-acetyl amide derivatives were semi-synthesized by treating 3-O-acetyl GA with oxalyl chloride (2equiv) in dry dichloromethane (DCM) for three hours followed by adding corresponding amines (1.5 equivalent) and triethylamine under nitrogen atmosphere (Figure 4b). The reaction mixture was stirred for four hours at room temperature. The reaction was quenched with H_2O (10 mL), and the organic phase was separated. The aqueous phase was extracted with CH_2Cl_2 (3x30 mL). The combined organic phase was dried over Na_2SO_4, filtered, and evaporated under vacuum to give the crude product. The products were purified by column chromatography, which afforded the desired derivatives. All the GA derivatives were characterized on the basis of their ^{1}H and ^{13}C NMR spectroscopic data.

Characterization of GL, GA and GA derivatives (GA1–GA5)

All the GA derivatives were characterized on the basis of their ^{1}H and ^{13}C NMR spectroscopic data as given below.

GL:

^{1}H NMR (300 MHz, C_5H_5N): δ 0.76 – 1.32 (3H each all s, 7 x tert.CH_3), 2.32 (s, 1 H; 9H), 1.97 (3H, s, C-32), 4.2 (1H, dd, J= 6.8 & 8.7 Hz, 3 α-H), 5.56 (1H, s, H-12), 5.20 (1H,d, H-1'), 3.23 (1H, m, H-2'), 3.62 (1H, m, H 3' & H-4'), 4.45 (1H, d, H-5'), 12.22 (1H, s, H-6'), 4.86 (1H,d, H-1"), 3.53 (1H, m, H-2", H-3" & H-4"), 4.5 (1H, d, H-5"), 12.3 (1H, s, H-6")

^{13}C NMR (C_5H_5N, 75MHz): 39.9 (C-1), 27.0 (C-2), 88.7 (C-3), 37.8 (C-4), 55.5 (C-5), 18.1 (C-6), 33.2 (C-7), 43.7 (C-8), 62.4 (C-9), 37.6 (C-10), 199.9 (C-11), 128.9 (C-12), 169.9 (C-13), 45.8 (C-14), 28.3 (C-15), 26.8 (C-16), 32.4 (C-17), 48.9 (C-18), 41.9 (C-19), 44.3 (C-20), 31.8 (C-21), 38.6 (C-22), 28.0 (C-23), 16.8 (C-24), 17.0 (C-25), 19.0 (C-26), 23.7 (C-27), 28.7 (C-28), 28.9 (C-29), 179.4 (C-30), 104.1 (C-1'), 83.1 (C-2'), 75.8 (C-3'), 71.7 (C-4'), 76.5 (C-5'), 170.5 (C-6'), 105.2 (C-1"), 75.4 (C-2"), 76.9 (C-3"), 71.8 (C-4"), 75.9 (C-5"), 170.6 (C-6").

GA:

^{1}H NMR (300 MHz, $CDCl_3$): δ 0.76 – 1.32 (3H each all s, 7 x tert.CH_3) 2.32 (s, 1 H, 9H), 3.36 (1H, dd, J= 6.8 & 8.5 Hz, 3 α-H) 5.62 (1H, m, H-12).

^{13}C NMR: 39.9 (C-1), 27.0 (C-2), 78.1 (C-3), 37.8 (C-4), 55.5 (C-5), 18.1 (C-6), 33.2 (C-7), 43.7 (C-8), 62.4 (C-9), 37.5 (C-10), 199.1 (C-11), 128.9 (C-12), 169.9 (C-13), 45.8 (C-14), 28.3 (C-15), 26.8 (C-16), 32.4 (C-17), 48.9 (C-18), 41.9 (C-19), 44.3 (C-20), 31.8 (C-21), 37.5 (C-22), 27.8 (C-23), 16.8 (C-24), 17.0 (C-25), 19.0 (C-26), 23.7 (C-27), 28.8 (C-28), 28.9 (C-29), 179.4 (C-30).

GA-1:

^{1}H NMR ($CDCl_3$, 300 MHz): δ 0.86-1.35 (3H each, all s, 7 x tert CH_3), 4.32 (1H, m, H-3), 5.61 (1H, s, H-12), 2.04 (3H, s, H-2').

^{13}C NMR ($CDCl_3$, 75MHz): δ_C 39.2 (C-1), 26.8 (C-2), 81.6 (C-3), 38.5 (C-4), 55.4 (C-5), 17.8 (C-6), 33.1 (C-7), 43.6 (C-8), 62.1 (C-9), 37.3 (C-10), 200.8 (C-11), 128.8 (C-12), 169.9 (C-13), 45.9 (C-14), 28.4 (C-15), 26.8 (C-16), 32.3 (C-17), 48.6 (C-18), 41.2 (C-19), 44.2 (C-20), 31.6 (C-21), 38.1 (C-22), 28.9 (C-23), 16.8 (C-24), 17.1 (C-25), 19.1 (C-26), 23.7 (C-27), 28.9 (C-28), 29.8 (C-29), 182.2 (C-30), 171.5 (C-1'), 21.7 (C-2').

GA-2:

^{1}H NMR ($CDCl_3$, 300 MHz): δ 0.83-1.34 (3H each, all s, 7 x tert CH_3), 4.48 (1H, m, H-3), 5.60 (1H, s, H-12), 2.00 (3H, s, H-2'), 3.24 (2H, m, H-1"), 0.86 (3H, t, *J* = 7.5 Hz, H-3").

^{13}C NMR ($CDCl_3$, 75MHz): δ 39.2 (C-1), 26.9 (C-2), 81.0 (C-3), 37.9 (C-4), 55.4 (C-5), 17.8 (C-6), 33.1 (C-7), 43.6 (C-8), 62.1 (C-9), 37.3 (C-10), 200.3 (C-11), 128.8 (C-12), 169.7 (C-13), 45.8 (C-14), 28.4 (C-15), 26.9 (C-16), 32.3 (C-17), 48.6 (C-18), 41.6 (C-19), 43.9 (C-

20), 31.9 (C-21), 38.4 (C-22), 28.9 (C-23), 16.7 (C-24), 17.0 (C-25), 19.1 (C-26), 23.7 (C-27), 28.9 (C-28), 30.0 (C-29), 176.0 (C-30), 171.3 (C-1'), 21.6 (C-2'), 42.3 (C-1"), 23.9 (C-2"), 11.8 (C-3").

GA-3:

^{1}H NMR ($CDCl_3$, 300 MHz): δ_C 0.85-1.37 (3H each, all s, 7 x tert CH_3), 4.46 (1H, m, H-3), 5.62 (1H, s, H-12), 2.02 (3H, s, H-2'), 3.29 (2H, m, H-1"), 0.85 (3H, t, *J* = 7.5 Hz, H-4").

^{13}C NMR ($CDCl_3$, 75MHz): δ_C 39.2 (C-1), 26.8 (C-2), 81.0 (C-3), 37.9 (C-4), 55.4 (C-5), 17.8 (C-6), 33.1 (C-7), 43.6 (C-8), 62.1 (C-9), 37.3 (C-10), 200.4 (C-11), 128.8 (C-12), 169.8 (C-13), 45.8 (C-14), 28.4 (C-15), 26.8 (C-16), 32.3 (C-17), 48.6 (C-18), 42.3 (C-19), 43.9 (C-20), 31.9 (C-21), 38.4 (C-22), 28.9 (C-23), 16.8 (C-24), 17.0 (C-25), 19.1 (C-26), 23.7 (C-27), 28.9 (C-28), 30.0 (C-29), 176.0 (C-30), 171.4 (C-1'), 21.7 (C-2'), 39.8 (C-1"), 33.1 (C-2"), 20.4 (C-3"), 14.0 (C-4").

GA-4:

^{1}H NMR ($CDCl_3$, 300 MHz): δ 0.84-1.40 (3H each, all s, 7 x tert CH_3), 4.79 (1H, dd, *J* = 6.3 & 8.9 Hz, H-3), 5.74 (1H, s, H-12), 7.47-8.13 (5H, m, Ar-H).

^{13}C NMR ($CDCl_3$, 75MHz): δ_C 39.2 (C-1), 26.8 (C-2), 81.7 (C-3), 38.2 (C-4), 55.5 (C-5), 17.8 (C-6), 32.3 (C-7), 43.6 (C-8), 62.2 (C-9), 37.4 (C-10), 200.6 (C-11), 128.9 (C-12), 172.5 (C-13), 45.9 (C-14), 28.6 (C-15), 26.8 (C-16), 31.3 (C-17), 48.6 (C-18), 38.9 (C-19), 45.9 (C-20), 30.1 (C-21), 37.4 (C-22), 28.9 (C-23), 16.8 (C-24), 17.4 (C-25), 19.1 (C-26), 23.8 (C-27), 28.9 (C-28), 29.8 (C-29), 176.0 (C-30), 172.5 (C-1'), 130.0 (C-2'), 130.6 (C-3'& C-7'), 128.9 (C-4'&C-6'), 133.1 (C-5').

GA-5:

^{1}H NMR ($CDCl_3$, 300 MHz): δ 0.99-1.35 (3H each, all s, 7 x tert CH_3), 4.48 (1H, m, H-3), 5.67 (1H, s, H-12), 2.04 (3H, s, H-2'), 3.82 (2H, t, *J* = 6.6 Hz, H-1"), 2.95 (2H, t, *J* = 6.6 Hz, H-2").

^{13}C NMR ($CDCl_3$, 75MHz): δ_C 39.2 (C-1), 26.8 (C-2), 80.6 (C-3), 38.0 (C-4), 55.4 (C-5), 17.8 (C-6), 33.1 (C-7), 43.7 (C-8), 62.2 (C-9), 37.4 (C-10), 201.0 (C-11), 128.7 (C-12), 171.4 (C-13), 45.9 (C-14), 28.4 (C-15), 26.8 (C-16), 32.2 (C-17), 48.6 (C-18), 41.9 (C-19), 44.1 (C-20), 30.1 (C-21), 38.4 (C-22), 29.0 (C-23), 16.8 (C-24), 17.1 (C-25), 19.1 (C-26), 23.7 (C-27), 28.4 (C-28), 29.9 (C-29), 177.0 (C-30), 171.4 (C-1'), 21.7 (C-2'), 45.9 (C-1"), 41.9 (C-2").

In-vitro cytotoxicity evaluation

Preparation of test sample solutions

The test samples 18β-glycyrrhetinic acid and its derivatives GA-1, GA-2, GA-3, GA-4 and GA-5 were weighed in micro centrifuge tubes and stock solutions of 20mM were made by dissolving the samples in DMSO. Stocks are stored at -20ºC. A working solution of 12.5, 25, 50, 100 and 200µM concentration was made by diluting the stock solution in culture medium.

Cell Culture

The MDA-MB-231 (Organism: Homo sapiens, Tissue/site: breast metastatic, Cell type: epithelial, TNBC) were procured from American Type Culture Collection (ATCC) and cultured as per manual instructions. The cells were cultured and maintained in RPMI-1640 medium at 37 ˚C and 5% CO2/95% air in a humidified incubator and were regularly examined microscopically for stable phenotype.

SRB Assay

Addition of cells: The cells were dispensed in a flat bottom 96-well plate. To each well, 100 µl of the cell suspension containing 10,000-15,000 ells were added. Further, the cells were incubated at 37 ºC in 5% CO2/95% air concentration for 24 h, prior to the addition of test samples.

Test samples addition: A working solution of 100 µl of test sample was added to the cell monolayer to give a final concentration 200µM. A series of four dilutions 12.5µM, 25µM, 50µM and 100µM for each derivative in three replicates were included.

Negative (Vehicle) Controls: In every assay plate DMSO was added in 0.1% concentration as vehicle control. The final concentration of DMSO was 0.1% in all assay wells. Finally, the plates were incubated at 37 ºC in 5% CO2 concentration for 48 h.

Addition of Sulphorhodamine B ass and colorimetric reading: Once the treatment period was done. After 48 h incubation, cold 50% trichloroacetic acid (TCA Sigma Aldrich, 50 µl/well) were added on top of the medium to fix the cells attached to substratum and incubated for one h at 4ºC. After that a five times gentle wash was given to the plate with slow running tap water to remove dead cells, culture medium and TCA. After washing, the plates were air dried. Further, 50 µl/well of SRB solution was added to the dried plate and left at room temperature for 30 min. After incubation, unbound SRB dye was removed by 4-5 times washing with 1 % (v/v) glacial acetic acid. Plates were allowed to air-dry at room temperature. Further, 150 µl of 10 mM Tris base solution was added to each well to solubilize the protein-bound dye, and plate is shaken for 15 min on a gyratory shaker. Finally, the absorbance was taken at 510 nm using a plate reader.

Data analysis

Percentage of cell growth inhibition in presence of the test sample is calculated as follows:

$$Percentage\ of\ cells\ killed = 100 - \left[\frac{MeanOD_{test}}{MeanOD_{control}}\right] + 100$$

Identification of therapeutic targets for GA in MDA-MB-231

Based on recently published report, a 48 hours treatment of MDA-MB-231 cells with 20µM/l GA attenuate cellular glutathione (GSH) level and cause apoptosis in TNBC cancers (Cai, *et al.*, 2017). The cellular GSH level is controlled by GLO-I and Topoisomerase-II as reported by Silva, *et al.*, 2013 & Cameron *et al.*, 1999. However, a web based target identification tools *viz.*, Stitch-DB (http://stitch.embl.de.) and Swiss target prediction identified, hydroxysteroid 11-beta-dehydrogenase-1(1HSD1) as possible binding targets for GA (Figure

S8, Supplementary information). Therefore, an approach of molecular docking based screening was applied for GA and derivatives to rank possible MDA-MB-231 targets *viz*., GLO-I, TOPO-II and 11HSD1 based on their degree of binding energies.

Molecular docking and atomic property field (APF) based scoring

The crystal structure of GLO-I (PDB: 4PV5) bound with glycyrrhetinic acid (2.3 resolution) was retrieved from protein database (Zhang, *et al*., 2015). The GA derivatives structures were converted to ICM object using ICM Molsoft–chemist v3.8-6, (2018) (Molsoft LLC, San Diego, USA). It uses Monte Carlo minimization in the atomic property field's potentials in conjunction with standard MMFF94 force-field energies. The method was developed by Totrov, 2008, 2011 & Grigoryan *et al.,* 2010. Protein-ligand docking tool FlexX provided by LeadIT software v2.1.6, 2017, (BioSolveIT GmbH, Sankt FeAugustin, Germany, www.biosolveit.de/LeadIT) was used to perform molecular interaction study as proposed procedure by Kramer, *et al.,* 1999. The amino acids within 10 Å region from GA active site of enzyme GLO-I were selected to get more flexibility in interaction study. Number of pose generation was set at 10 and computed pose with minimum energy (RMSD) was selected for comparative study.

Computational assessment for oral bioavailability and toxicity

All the five GA derivatives were also studied for their oral bioavailability by calculating various pharmacokinetic parameters such as plasma protein binding, blood brain barrier penetration capacity, intestinal absorption, hepatotoxicity, oral bioavailability. Furthermore, the derivatives were evaluated for toxicity risk screening using Discovery Studio v3.5 TOPKAT (Toxicity Prediction by Komputer Assisted Technology) tool. TOPKAT is a Quantitative Structure Toxicity Relationship (QSTR) based tool developed by Accelrys Inc. USA (http://accelrys.com) licensed to CSIR-CIMAP, Lucknow (www.cimap.res.in). The module utilizes highly robust and cross-validated QSTR models to predict toxicity. The module applies patented Optimal Predictive Space (OPS) which is a unique multivariate descriptor space for result interpretation (Enslein, *et al.,* 1988, 1987). The module computes the toxic and environmental effects of compounds exclusively from their chemical structures. DS-TOPKAT module search fragments within query molecule based on molecular fingerprint similarity with the training set compounds. The TOPKAT toxicity prediction results for unknown compound are calculated based on Probability score, Bayesian scores and Mahalanobis distance (structure similarity) from the centre of the training set compounds. DS-TOPKAT gives predictions for a range of toxicological endpoints, including mutagenicity, developmental toxicity, rodent carcinogenicity, rat chronic Lowest Observed Adverse Effect Level (LOAEL), rat Maximum Tolerated Dose (MTD) and rat oral LD_{50} (Table S6, Supplementary material).

Results and Discussion

2D-QSAR model development and validation results

The developed quantitative structure–activity relationship model (QSAR) identifies activity inducing features of 144 MDA-MB-231 inhibitors selected in the model development (Table S1 and S2, Supplementary material). The developed QSAR model was validated through

various statistical approaches *viz*., leave-one-out (LOO), external test set prediction (r^2_{pred}), Z-scores and r_m^2 matrix calculation. The results of statistical parameters are summarized in Table 1.

QSAR multiple linear regression equation

PIC_{50} (μM) = 0.0016 +7.2421 (Epsilon4) +1.2894 (chiV3Cluster) -0.7603 (T_N_N_5) +0.1635 (Nitrogen count) +2.3425 (chi3chain) (**Equation 6**)

Where, N (training set, 70% of 144 MDA-MB-231 inhibitors) = 100, n (test set, 30% of 144 MDA-MB-231 inhibitors) =44, r2 (Regression coefficient for training set) =0.8442, R2se=0.3063, q2 (Regression coefficient for leave one out (LOO) validation) =0.8282, q2se= 0.3214, Fisher test = 101.6555, predicted r2 (Regression coefficient for external test set) =0.7532, pred r2se= 0.3659, Z score R^2= 14.76689, Z score q^2 = 14.61679 and Z score pred r^2 = 4.11170

The QSAR model attain good correlation coefficient of 0.84 for training set of 100 inhibitors. The fitness plot between observed and predicted PIC_{50} values is presented in Figure 5. The high value of cross validation (LOO) regression (q^2), 0.82 indicates training set compounds (blue dots) exhibit less statistical noise. Regression coefficient for random selected 44 external test set (Pred R^2) was found 0.75. The test set regression infers the good predictability of model for unknown compounds (red dots), a small measure of error (0.0016) indicate data comprehensiveness. Additionally, an even distribution of residual values around the axis line indicate good model quality (Figure S3, Supplementary material). Furthermore, high value for Fishers test, F= 101.65, again verified robustness of the model. Also, a high Z scores of 14.76689, 14.61679 and 4.11170 for r^2, q^2 and pred r^2 respectively, supported the good model quality. The computed statistical qualities for training and test sets are summarized in Table 1 and Table 2 with their reported cut off values.

Based on Ojha, *et al*., 2011 the r^2_{pred} is not a true evidence for model prediction ability. Since, r^2_{pred} depends on training set mean and therefore greatly influenced by training set and test set selection. However, r_m^2 matrix shows the predictability of the model for whole dataset. For test set the acceptable range for parameters, r^2_{pred}, r_m^2 and r'^2_m is 0.5, Δr_m^2 should be less than 0.2 and r^2_{mbar} should be more than 0.5 (Ojha, *et al*., 2011). In the present case the r^2, r^2 (LOO), r_m^2 r'^2_m, r^2_{mbar} and Δr_m^2 values for training set are 0.84, 0.82, 0.83, 0.71, 0.77 and 0.11 respectively (Table 1). All statistical parameters for training set were found within their cut off limits (Table 1). For test set, r^2_{pred}, r_m^2 and r'^2_m were found 0.75, 0.67 and 0.63 respectively. The calculated values of $r^2_{m\ (bar)}$ and Δr_m^2 for test set are 0.65 and 0.03 respectively that are within their cut off limits (Table 2). The computed r^2_m matrix validate

the reliability and robustness of developed QSAR model for anticancer activity prediction of unknown compounds. Also, the model identified features help to explore the structure based inhibition mechanism of MDA-MB-231inhibitors.

QSAR model identified 2D structural properties and description

Generated equation 6 explains the model extracted out five important descriptors that determine the cytotoxic potential of MDA-MB-231 inhibitors are (i) Epsilon4 that signified measure of electronegativity count, (ii) ChiV3cluster indicate valence molecular connectivity index, (iii) chi3chain represents retention index for three membered ring, (iv) TNN5 stands for nitrogen atoms separated through 5 bond distances and (v) nitrogen counts *i.e*., number of nitrogen atoms in the molecule.

The topochemical descriptor Epsilon4 signifies measure of electronegativity count and contributing 11% to the biological activity (PIC_{50}). The descriptor chiV3Cluster, belong to valence molecular connectivity index of 3rd order cluster (Shen, *et al.,* 2002). It is known that molecular connectivity indices are most successful among other topological properties in compound property estimation. Since these indices are based on contingent chemical, structural and mathematical ground. The important advantage of the molecular connectivity model comprises its flexibility, to quantify general as well as local structural properties. The percentage contribution for identified descriptors are presented in figure S4 under supplementary material. Figure S4 describes descriptor chiV3Cluster contribute 30% to biological activity of training set compounds. Whereas, TNN5 descriptor that define two nitrogen atoms separated through 5 bond distances, showed inverse relationship to the biological activity. However, descriptor nitrogen count is showing positive effect and contributing 21% to the activity (PIC_{50}). Additionally, the equation 6 indicate nitrogen containing functional groups may increase the biological activity. Though chemical fragments containing nitrogen atoms departed by long chain (TNN5) might not be very favourable. Overall, the model suggests maximum contribution hail from the descriptors chiV3Cluster, Epsilon4 and nitrogen count (Figure S4, supplementary material).

2D-QSAR model AD assessment results

A PCA analysis indicates 44 test set compounds fall within the structure space of training set compounds. Figure 6 shows generated PCA graph for training set (blue sphere) and test set (yellow sphere). The figure illustrates a uniform distribution of test set within the vector space of training set compounds. The figure defines the test set as a true representative of training set. Also, a broad biological activity space of 10^{-1} to 10^{1} µM for training and test set indicate the data was comprehensive. A correlation matrix for PIC_{50} and extracted descriptor (Epsilon4, chiV3Cluster, T_N_N_5, Nitrogen count and chi3chain) was also generated (Table S4, Supplementary materials). It showed that the developed model based on the selected descriptors is well established.

A UPGMA based hierarchical cluster analysis (Tanimoto structure similarity distance 0-0.7) of 144 dataset compounds indicate that training set, test and five GA derivatives come within the applicability domain of QSAR model. Also, the heat map generation for chemical properties *viz.,* molecular weight, logP, polar surface area, maximum ring size, minimum ring

size, maximum fused rings, and number of rotatable bonds also indicate the optimal chemical property range (Figure S1, Supplementary material).

Identified 3D structural property fields through 3D-QSAR studies

At this point, an attempt was made to generate APF based 3D-QSAR analysis to systematically describe the structural atomic field level of novel GA derivatives. The 3D-QSAR analysis performed by Atom Property Fields (APF) methods was developed by Totrov, *et al.*, 2008. For this purpose, a set of congeneric series of 42 GA derivatives, with *in-vitro* inhibition activity against MDA-MB-231 cell line were selected. The dataset structures were flexibly aligned to the generated property fields of co-crystallised GA on GLO-I. The co-crystallised GA on GLO-I binding site is depicted in Figure 7. The generated model presented a good regression coefficient of 0.96 for training set compounds. Also, the external test set based regression reverted a good predictive regression coefficient of 0.82 (Table 3, Table 4). The regression plot between observed and predicted PIC_{50} for training and test sets are showed in figure 8 and figure 9. The calculated results of statistical parameters training and test sets are compiled in Table 3 and Table 4 respectively. All statistical properties were found within their cut off limit. The results indicate generated model is robust enough to give consistent prediction for novel GA derivatives. Henceforth, novel GA compounds namely GA-1, GA-2, GA-3, GA-4 and GA-5 were aligned on training and their PIC_{50} values were predicted through developed 3D-QSAR model. The model presented IC_{50} for GA derivatives ranges from 44.26 µM to 103.75 µM. Based on 3D-QSAR model predicted results it has been expected that designed derivatives may show moderate activity against TNBC cell line.

Semi-synthesis and SRB based in-vitro cytotoxicity assay results for GA derivatives GA-1, GA-2, GA-3, GA-4 and GA-5 against metastatic TNBC cell line MDA-MB-231

Our design concept for GA derivatives, GA-1, GA-2, GA-3, GA-4 and GA-5 was to introduce structural variations at C-3 and C-30 positions to improve the anticancer efficiency. The 2D QSAR model extracted descriptor Epsilon4 indicate electronegativity on GA cause favourable effects on biological activities. A positive correlation with electronegativity was also found in 3D-QSAR studies (Figure 10). 2D-QSAR descriptor ChiV3cluster suggested less branching at GA scaffold is favourable. Hence, small fragments *viz.*, propyl amide, butyl amide and amino ethyl amide were substituted at C-30 carbon (GA-1, GA-2, GA-3 and GA-5). The structures of prepared derivative are given in Figure 4a and Figure 4b. However, 3D QSAR based property fields suggest lipophilicity and electronegativity are playing governing role in anticancer properties of GA derivatives. Therefore, a derivative with benzoate group substitution at C-3 position was also prepared (GA-4). The detailed analysis of 2D and 3D QSAR based structure activity relationship is illustrated in Figure 10. Based on QSAR model studies five novel derivatives of GA named GA-1, GA-2, GA-3, GA-4 and GA-5 were semi-synthesised with modifications at C-3 and C-30 positions and screened through the developed model (Figure 4a, 4b).

Further, a dose dependent *in-vitro* cytotoxicity of GA and derivatives were investigated against metastatic TNBC cell line MDA-MB-231. The 48 hours exposure of derivatives GA-1, GA-3 and GA-4 inhibit MDA-MB-231 cells with IC_{50} 76.5 µM, 91.79 µM and 116.07 µM respectively (Table 5). Derivative GA-1 was found most active as it showed most cytotoxic activity against MDA-MB-231 cells. However, GA-2 and GA-5 were found least effective as they indicated 35.56% and 25.63% cancer cells inhibition at maximum concentration of 200µM. GA-3 and GA-4 showed moderate inhibition potentials of 91.79 µM and 116.07 µM respectively.

2D and 3D-QSAR model results and their correlation with in-vitro activity of GA-1, GA-2, GA-3, GA-4 and GA-5

In order to prospectively validate the generated 2D and 3D QSAR models the anticancer activities of the novel GA derivatives were calculated and compared with the *in-vitro* activity. Relevance for 2D-QSAR was based on the data homogeneity constructed using natural scaffold-based training set with fused rings structures (2-5 rings) (Figure S3, supplementary material). The GA derivatives are pentacyclic triterpene. The 2D QSAR model predicted IC_{50} was in the range of 49 µM to 18 µM. No much difference in activities between GA-1, GA-2 and GA-3 was predicted because of their high topological similarity. Hence, an Atomic potential field based 3D QSAR was applied to recognize biologically significant structural features of GA derivatives. The dataset for 3D-QSAR was based on congeneric series of GA derivatives. Consequently, it has been expected that APF based 3D QSAR model might present more specific results for derivatives. The model presented IC_{50} for GA derivatives ranges from 44.26 µM to 103.75 µM. The 3D QSAR prediction provided more variations in PIC_{50} of GA derivative. Also, a positive correlation between APF scores and *in-vitro* activity indicate correlation between atomic property fields score in negative and cytotoxic activity (Figure 11).

The results of 2D and 3D QSAR models and *in-vitro* activities on GA derivatives indicate 3-*O*-acyl derivative named GA-1 was more significant in terms of biological activity. It has been found that modification at C-30 carboxylic group with amide group in GA-2, GA-3, GA-4 and GA-5 resulted decrease in cytotoxic potential against MDA_MB-231. Moreover, APF 3D QSAR based predicted activities for derivatives were found comparable to their *in-vitro* IC_{50} values. Therefore, the results indicate APF based 3D QSAR performed well in predicting the biological activities of studied compounds.

Mode of action study, binding energy and APF scores of GA-1, GA-2, GA-3, GA-4 and GA-5 with anticancer target GLO-I

Breast cancer majorly depends on glycolysis as energy source based on Warburg effect (Sullivan, *et al.,* 2016; Fonseca-Sánchez, *et al.,* 2012). During glycolysis a highly reactive compound known as methyl glyoxalases are formed. GLO-I metabolize and inactivate methylglyoxlase produced through glycolysis, making GLO-I inhibitors as potential anti-tumor agents (Cai, *et. al.,* 2016, Silva, *et. al.,* 2013). Inhibition of GLO-I resulted in the accumulation of α-oxoaldehydes at cytotoxic levels and reverse multi drug resistance (MDR). RT-PCR, western blot analysis of metastatic breast cancer MDA-MB-231 often show high expression of GLO-I. Additionally, knockdown study on GLO-I enzyme supress migration,

invasion and promote apoptosis in metastatic breast cancer cells (Guo, *et al.*, 2016). Conventional and most considered GLO-I inhibitors are coenzyme GSH analogs, which exhibits efficient inhibition *in-vitro* (Silva, *et. al.*, 2013) and reverse MDR, thus GLO-I inhibitors have been proposed as efficient anti-tumor agents. However, these GSH based inhibitors suffer from poor pharmacokinetic properties and are difficult to use as lead structure for the further design of small molecule. Alternatively, non-GSH analog natural inhibitors include flavonoids, methylgerfelin (MGI), indomethacine, zopolrestat and curcumin and its derivatives showed good pharmacokinetic properties (Zhang, *et al.*, 2015). Notably the carboxylic group of these molecules mimic, glycyl and γ-glutamyl residue moieties of GSH to form hydrogen bonds with the glycyl and glutamyl sites, respectively, in the GSH binding site (Figure S5, Supplementary material). Recently, Cai, *et al*., (2017) has reported MDA-MB-231 treatment with 20 μM/l of GA for 48 hour which causes apoptosis by inducing GSH inhibition.

Here, a docking based screening of GA derivatives presented good binding energy with predicted target GLO-I in comparison to other two targets 11HSD1 and TOPO-II (Table S5, Supplementary material). Therefore, a non GSH based ligand namely GA-1, GA-2, GA-3, GA-4 and GA-5 were analysed for their binding affinity towards GLO-I enzyme.

The mammalian GLO-I exhibit two binding sites with zinc as a cofactor at its catalytic binding site. One of the binding sites is glycyl site specific for GSH binding as presented in Figure 7. The key amino acid residues for glycyl site are LYS150A, GLY155A, LYS156A, and LEU160A AND PHE162A. However, glutamyl site exhibited key amino acids, ARG37B, ASN103B and ARG122A. While the Zn^{2+} catalytic site coordinating residues include GLN32, HIS126 and GLU172. As reported by Zhang, *et al.* (2015) for a non-GSH analogs GA doesn't require metal Zn^{2+} coordination. Therefore, in the present work Zinc ion was excluded while docking process as GA is a pentacyclic triterpenoid. From the APF based alignment and scoring, it is evident that carboxylic group at C-30 position plays a critical role in GA-GLO-I binding. The C-30 carboxylic group hydrogen atom is highly polar and cause negative charge over oxygen after ionization. This leads to hydrogen bonding between C-30 - $RCOO^-$ with polarized hydrogen atoms present in amino acid residues ARG-38 (1.8 Å) and ASN-104 (2.3 Å) (electrophilic centres) of GLO-I binding pocket.

In accordance with the results the most active GA derivative GA-1 (IC_{50} = 76.5 μM) showed highest APF score of -425.82 (Figure 11). For this purpose, the parent compound GA with APF -219.67 (IC_{50} = 82.29) was taken as positive control to identify structure-activity relationship based on their APF score. The least active derivatives GA-2 (IC_{50} >200 μM) and GA-5 (IC_{50} >200 μM) showed minimum APF score of -402.047 and -402.14. Likewise, derivative GA-3 and GA-4 with moderate IC_{50} of 91.79 μM and 116.07 μM accordingly presented a moderate APF score of -401.18 and -415.68. Consequently, the APF alignment score and IC_{50} values indicated that the carboxylic group at C-30 in GA-1 and GA-4 in some way play a major role in enzyme receptor binding.

Footnote: *Atomic property field (APF) based score calculated through ICM-Chemist v3.-6a (Molsoft L.L.C., USA, licensed to CSIR-CIMAP, Lucknow, India)

Correspondingly, the FlexX based binding energy calculation of GA derivatives on GLO-I was also found in close agreement with APF guided structure-based screening results (Table 6). The results of molecular docking of GA and its derivatives against GLO-I approved that GA-1 exhibited highest binding affinity of -16.997 kJ/mol in comparison to derivatives GA-2 (-9.7 kJ/mol), GA-3 (-7.293 kJ/mol), GA-5 (-10.419 kJ/mol). However, GA-4 also showed good binding affinity (-21.232 kJ/mol). The binding pose analysis of active GA-1 showed amino acid residues ARG-38 and ARG-123 form hydrogen bonds with C-30 carboxylic group of GA-1. The proposed binding pose of GA-1 on GSH binding site of GLO-I is represented in figure 13.

Oral bioavailability and toxicity risks assessment results

Rodent (mouse/rat) carcinogenic probability based on data from National Toxicological programme (NTP) showed GA and its derivatives as non-carcinogen. Conversely, the US Food and Drug Administration (FDA) based data predicted GA and its derivatives as carcinogenic compounds. This contraindication was resolved by considering Weight Of Evidence (WOE) prediction that indicate GA and its derivatives may possess carcinogenic character. Many anticancer compounds often possess carcinogenic characters since they target proliferating cells and cause developmental toxicity in developing embryos. However, Ames mutagenic prediction showed derivatives as non-mutagenic. Here, GA-1, GA-2 and GA-3 were also found non-toxic for developmental mutagenicity. Additionally, GA-1 showed moderate to severe skin effect and ocular irritancy. Detail compliance for computational toxicity analysis are provided in supplementary table S6. Lastly, the computational results showed that GA and its derivatives have good aerobic biodegradability, hence they are non-persistent and safe to the environment.

Conclusions

In this study the QSAR model predicted IC_{50} and SRB assay based biological activities of GA derivatives, GA-2, GA-3, and GA-4 were found comparable against triple negative breast cancer cell line MDA-MB-231. This indicated that the model extracted structural features *viz*., Epsilon4 (measure of electronegativity count), ChiV3cluster (valence molecular connectivity index), chi3chain (retention index for three membered ring), TNN5 (nitrogen atoms separated through 5 bond distances) and nitrogen counts had significant contribution to the biological activity. The results also signify that OH group substitution with acyl group at C-3 position increases the compound lipophilicity thereby increasing the cytotoxicity potential against TNBC breast cancer cell line MDA-MB-231. Conversely, substitution at C-30 position with propyl amide, butyl amide and amino ethyl amide resulted in decreased cytotoxicity. However, C-30 substitution with butyl amide did not cause any significant difference. Whereas the cytotoxicity was decreased due to addition of benzoate group at C-3 position. Over all the results suggested that C-30 carboxylic group is crucial for GA based cytotoxic activity. Therefore, an addition of 3-O-acetyl group at C-3 increases GA lipophilicity thereby improves the cytotoxicity.

Additionally, APF based scoring and FlexX based binding affinity with GLO-I, a highly expressing enzyme in metastatic TNBC breast cancers confirmed that GA and GA-1 exhibited maximum binding affinity. APF based flexible alignment of GA-1 with co-crystallized GA again established the significance of C-30 carboxyl group as it serves to

make three hydrogen bonds with GLO-I key amino acids ARG-38, ARG-123 and ASN-104. Thus, it's a novel work reporting active natural leads screened virtually using different molecular modelling approaches and *in-vitro* validation of predicted results tested on triple negative breast cancer cell lines. This study will be helpful in early lead discovery against metastatic breast cancers.

Author's contribution

AS, FK and SKS designed the detailed experiments, performed the study, and collected and analyzed the data. RK and SKS synthesised and characterised the derivatives. SM and DD performed *in-vitro* SRB assay. All authors analysed the results and approved the final manuscript.

Acknowledgment

AS acknowledges the Department of Science & Technology (DST), Govt. of India, New Delhi for financial assistance through WOS-B fellowship (GAP-339; S.No. DST/KIRAN/SoRF-PM/007/2015/CG) at CSIR-CIMAP. SKS acknowledges the Indian Council of Medical Research (ICMR), New Delhi for the Emeritus Medical Scientist at CSIR-CIMAP, Lucknow. We are also thankful to the Director, CSIR-CIMAP, Lucknow, India for rendering essential research facilities and support. We acknowledges Jawaharlal Nehru University (JNU), New Delhi for Ph.D registration and administrative support. The CIMAP communication number is CIMAP/PUB/2018/40.

Conflict of interest

All authors declare no conflict of interest.

References

Polyak, K. (2011) Heterogeneity in breast cancer. The Journal of clinical investigation, 121(10), 3786-3788. DOI: 10.1172/JCI60534.

Ovcaricek, T.; Frkovic, S.; Matos, E.; Mozina, B.; & Borstnar, S. Triple negative breast cancer-prognostic factors and survival. Radiology and oncology, 2011, 45(1), 46-52. DOI: 10.2478/v10019-010-0054-4.

Bianchini, G., Balko, J. M., Mayer, I. A., Sanders, M. E., & Gianni, L. (2016). Triple-negative breast cancer: Challenges and opportunities of a heterogeneous disease. Nature Reviews Clinical Oncology, 13(11), 674-690. DOI: 10.1038/nrclinonc.2016.66.

Thike, A. A., Cheok, P. Y., Jara-Lazaro, A. R., Tan, B., Tan, P., & Tan, P. H. (2010). Triple-negative breast cancer: clinicopathological characteristics and relationship with basal-like breast cancer. Modern pathology, 23(1), 123. DOI: 10.1038/modpathol.2009.

Zardavas, D.; Baselga, J.; Piccart, M. (2013) Emerging targeted agents in metastatic breast cancer. Nature reviews Clinical oncology, 2013, 10(4), 191. DOI: 10.1038/nrclinonc.2013.29.

Iqbal, J.; Abbasi, B.A.; Batool, R.; Mahmood, T.; Ali, B.; Khalil, A.T.; Kanwal, S.; Shah, S.A.; Ahmad, R. (2018) Potential phytocompounds for developing breast cancer therapeutics:

Nature's healing touch. European Journal of Pharmacology, 827: 125-148. DOI: 10.1016/j.ejphar.2018.03.007.

Jamdade, V. S.; Sethi, N.; Mundhe, N. A.; Kumar, P.; Lahkar, M.; Sinha, N. (2015) Therapeutic targets of triple-negative breast cancer: a review. British journal of pharmacology, 172(17), 4228-4237. DOI: 10.1111/bph.13211.

Wein, L.; Luen, S. J.; Savas, P.; Salgado, R.; Loi, S. (2018) Checkpoint blockade in the treatment of breast cancer: current status and future directions. British journal of cancer, 119(1). DOI: 10.1038/s41416-018-0126-6.

Badve, S.; Dabbs, D. J.; Schnitt, S. J.; Baehner, F. L.; Decker, T.; Eusebi, V.; Fox, S.B.; Ichihara, S.; Jacquemier, J.; Lakhani, S.R.; Palacios, J. (2011) Basal-like and triple-negative breast cancers: a critical review with an emphasis on the implications for pathologists and oncologists. Modern Pathology, 24(2), 157. DOI: 10.1038/modpathol.2010.200.

Tewari, D.; Mocan, A.; Parvanov, E. D.; Sah, A. N.; Nabavi, S. M.; Huminiecki, L.; Ma, Z.F.; Lee, Y.Y.; Horbańczuk, J.O.; Atanasov, A.G. (2017) Ethnopharmacological Approaches for Therapy of Jaundice: Part II. Highly Used Plant Species from Acanthaceae, Euphorbiaceae, Asteraceae, Combretaceae, and Fabaceae Families. Frontiers in Pharmacology, 8, 519. DOI: 10.3389/fphar.2017.00519.

Krähenbühl, S.; Hasler, F.; & Krapf, R. (1994) Analysis and pharmacokinetics of glycyrrhizic acid and glycyrrhetinic acid in humans and experimental animals. Steroids, 59(2), 121-126. DOI: org/10.1016/0039-128X (94)90088-4.

Negishi, M.; Irie, A.; Nagata, N.; Ichikawa, A. (1991) Specific binding of glycyrrhetinic acid to the rat liver membrane. Biochimica et Biophysica Acta (BBA)-Biomembranes, 1066(1), 77-82. DOI:org/10.1016/0005-2736(91)90253-5.

Cai, Y.; Xu, Y.; Chan, H. F.; Fang, X.; He, C.; Chen, M. (2016) Glycyrrhetinic acid mediated drug delivery carriers for hepatocellular carcinoma therapy. Molecular pharmaceutics, 13(3), 699-709. DOI: 10.1021/acs.molpharmaceut.5b00677.

Yadav, D.K.; Kalani, K., Singh, A.K.; Khan, F.; Srivastava, S.K.; Pant, A.B. (2014), Design, synthesis and in vitro evaluation of 18β-glycyrrhetinic acid derivatives for anticancer activity against human breast cancer cell line MCF-7. Current medicinal chemistry, 21(9), 1160-1170. DOI: 10.2174/1573406411309080009.

Yadav, D.K.; Kalani, K.; Khan, F., & Kumar Srivastava, S. (2013). QSAR and docking based semi-synthesis and in vitro evaluation of 18 β-glycyrrhetinic acid derivatives against human lung cancer cell line A-549. *Medicinal Chemistry*, *9*(8), 1073-1084. DOI: 10.2174/1573406411309080009

Yadav, D. K.; & Khan, F. (2013). QSAR, docking and ADMET studies of camptothecin derivatives as inhibitors of DNA topoisomerase- I. *Journal of chemometrics*, *27*(1-2), 21-33. DOI: org/10.1002/cem.2488.

Goldbrunner, M.; Loidl, G.; Polossek, T.; Mannschreck, A.; von Angerer, E. (1997) Inhibition of tubulin polymerization by 5, 6-dihydroindolo [2, 1-a] isoquinoline derivatives. Journal of medicinal chemistry, 40(22), 3524-3533. DOI: 10.1021/jm970177c.

Gao, C.; Dai, F. J.; Cui, H. W.; Peng, S. H.; He, Y.; Wang, X.; Qiu, W. W. (2014) Synthesis of Novel Heterocyclic Ring-Fused 18β-Glycyrrhetinic Acid Derivatives with Antitumor and Antimetastatic Activity. Chemical biology & drug design, 84(2), 223-233. DOI: 10.1111/cbdd.12308.

He, S.; Dong, G.; Wang, Z.; Chen, W.; Huang, Y.; Li, Z.; Zhang, W. (2015) Discovery of novel multiacting topoisomerase I/II and histone deacetylase inhibitors. ACS medicinal chemistry letters, 6(3), 239-243. DOI: 10.1021/ml500327q.

Li, Y.; Feng, L.; Song, Z. F.; Li, H. B.; & Huai, Q. Y. (2016). Synthesis and anticancer activities of glycyrrhetinic acid derivatives. *Molecules*, *21*(2), 199. DOI: 10.3390/molecules21020199

Motiwala, H. F.; Bazzill, J.; Samadi, A.; Zhang, H.; Timmermann, B. N.; Cohen, M. S.; Aubé, J. (2013) Synthesis and cytotoxicity of semisynthetic withalongolide A analogues. ACS medicinal chemistry letters, 4(11), 1069-1073. DOI: 10.1021/ml400267q.

Cramer III, R. D., Bunce, J. D., Patterson, D. E., & Frank, I. E. (1988). Crossvalidation, bootstrapping, and partial least squares compared with multiple regression in conventional QSAR studies. Quantitative Structure- Activity Relationships, 7(1), 18-25. DOI: org/10.1002/qsar.19880070105.

Golbraikh, A.; Tropsha, A. Beware of q2!. Journal of molecular graphics and modelling, 2002, 20(4), 269-276. DOI: org/10.1016/S1093-3263 (01)00123-1.

Ojha, P. K..; Mitra, I.; Das, R. N.; & Roy, K. (2011). Further exploring rm2 metrics for validation of QSPR models. *Chemometrics and Intelligent Laboratory Systems*, *107*(1), 194-205. DOI.org/10.1016/j.chemolab.2011.03.011.

Shen, M.; LeTiran, A.; Xiao, Y.; Golbraikh, A.; Kohn, H.; Tropsha, A. (2002) Quantitative structure− activity relationship analysis of functionalized amino acid anticonvulsant agents using k nearest neighbor and simulated annealing PLS methods. Journal of medicinal chemistry, 45(13), 2811-2823. DOI: 10.1021/jm010488u.

Kier, L.B.; Hall, L.H. (1977) Nature of structure-activity-relationships and their relation to molecular connectivity. European Journal of Medicinal Chemistry, 12 (4), 307-312.

Zheng, W.; Tropsha, A. (2000) Novel variable selection quantitative structure− property relationship approach based on the k-nearest-neighbor principle. Journal of chemical information and computer sciences, 40(1), 185-194. DOI: 10.1021/ci980033m.

Roy, K.; Ambure, P.; Kar, S. & Ojha, P. K. (2018). Is it possible to improve the quality of predictions from an "intelligent" use of multiple QSAR/QSPR/QSTR models? *Journal of Chemometrics*, *32*(4), e2992. DOI.org/10.1002/cem.2992.

Jaworska, J.; Nikolova-Jeliazkova, N.; & Aldenberg, T. (2005). QSAR applicability domain estimation by projection of the training set descriptor space: a review. *ATLA-NOTTINGHAM-*, *33*(5), 445.

Adhikari, N.; Amin, S. A.; Jha, T., & Gayen, S. (2017). Integrating regression and classification-based QSARs with molecular docking analyses to explore the structure-antiaromatase activity relationships of letrozole-based analogs. Canadian Journal of Chemistry, 95(12), 1285-1295. DOI.org/10.1139/cjc-2017-0419.

Amin, S. A.; Bhargava, S.; Adhikari, N.; Gayen, S., & Jha, T. (2018). Exploring pyrazolo [3, 4-d] pyrimidine phosphodiesterase 1 (PDE1) inhibitors: a predictive approach combining comparative validated multiple molecular modelling techniques. *Journal of Biomolecular Structure and Dynamics*, *36*(3), 590-608. DOI: org/10.1080/07391102.2017.1288659.

Abagyan R (2018) http://www.molsoft.com/icm-chemist-pro.html

Totrov, M. (2008) Atomic property fields: generalized 3D pharmacophoric potential for automated ligand superposition, pharmacophore elucidation and 3D QSAR. Chemical biology & drug design, 71(1), 15-27. DOI: org/10.1111/j.1747-0285.2007.00605.x.

Totrov, M. (2011) Ligand binding site superposition and comparison based on Atomic Property Fields: identification of distant homologues, convergent evolution and PDB-wide clustering of binding sites. BMC bioinformatics, 12(1), S35. DOI: 10.1186/1471-2105-12-S1-S35.

Cai, Y.; Zhao, B.; Liang, Q.; Zhang, Y.; Cai, J.; & Li, G. (2017). The selective effect of glycyrrhizin and glycyrrhetinic acid on topoisomerase IIα and apoptosis in combination with etoposide on triple negative breast cancer MDA-MB-231 cells. European journal of pharmacology, 809, 87-97. DOI: org/10.1016/j.ejphar.2017.05.026.

Silva, M. S.; Gomes, R. A.; Ferreira, A. E.; Freire, A. P.; Cordeiro, C. (2013) The glyoxalase pathway: the first hundred years and beyond. Biochemical Journal, 453(1), 1-15. DOI: 10.1042/BJ20121743.

Cameron, A.D.; Ridderström, M.; Olin, B.; Kavarana, M.J.; Creighton, D.J.; Mannervik, B. (1999) Reaction mechanism of glyoxalase I explored by an X-ray crystallographic analysis of the human enzyme in complex with a transition state analogue. Biochemistry. 38: 13480–90. DOI: 10.1021/bi990696c

Zhang, H.; Huang, Q.; Zhai, J.; Zhao, Y. N.; Zhang, L. P.; Chen, Y. Y.; Hu, X. P. (2015) Structural basis for 18-β-glycyrrhetinic acid as a novel non-GSH analog glyoxalase I inhibitor. Acta Pharmacologica Sinica, 36(9), 1145. DOI:10.1038/aps.2015.59.

Grigoryan, A. V.; Kufareva, I.; Totrov, M.; Abagyan, R. A. (2010) Spatial chemical distance based on atomic property fields. Journal of computer-aided molecular design, 24(3), 173-182. DOI: 10.1007/s10822-009-9316-x.

Kramer, B.; Rarey, M.; Lengauer, T. (1999) Evaluation of the FLEXX incremental construction algorithm for protein–ligand docking. Proteins: Structure, Function, and Bioinformatics, 37(2), 228-241. DOI: org/10.1002/(SICI)1097-0134(19991101).

Enslein, K. (1988). An overview of structure-activity-relationships as an alternative to testing in animals for carcinogenicity, mutagenicity, dermal and eye irritation, and acute oral toxicity. Toxicology and Industrial Health, 4,479-498. DOI: org/10.1177/074823378800400407.

Enslein, K.; Borgstedt, H. H.; Blake, B. W.; Hart, J. B. (1987) Prediction of rabbit skin irritation severity by structure activity relationships. In Vitro. Toxicology, 1, 129-147.

Sullivan, L. B.; Gui, D. Y.; Vander Heiden, M. G. (2016). Altered metabolite levels in cancer: implications for tumour biology and cancer therapy. Nature Reviews Cancer, 16(11), 680. DOI:.org/10.1038/nrc.2016.85.

Fonseca-Sánchez, M.A.; Rodríguez Cuevas, S.; Mendoza-Hernández, G.; Bautista-Piña, V.; Arechaga Ocampo, E.; Hidalgo Miranda, A.; Quintanar Jurado, V.; Marchat, L.A.; Álvarez-Sánchez, E.; Pérez Plasencia, C.; López-Camarillo, C. (2012). Breast cancer proteomics reveals a positive correlation between glyoxalase 1 expression and high tumor grade. International journal of oncology, 41(2), pp.670-680. DOI: org/10.3892/ijo.2012.1478.

Guo, Y.; Zhang, Y.; Yang, X.; Lu, P.; Yan, X.; Xiao, F.; Zhou, H.; Wen, C.; Shi, M.; Lu, J.; Meng, Q.H. (2016). Effects of methylglyoxal and glyoxalase I inhibition on breast cancer cells proliferation, invasion, and apoptosis through modulation of MAPKs, MMP9, and Bcl-2. Cancer biology & therapy, 17(2), pp.169-180. DOI: 10.1080/15384047.2015.1121346.

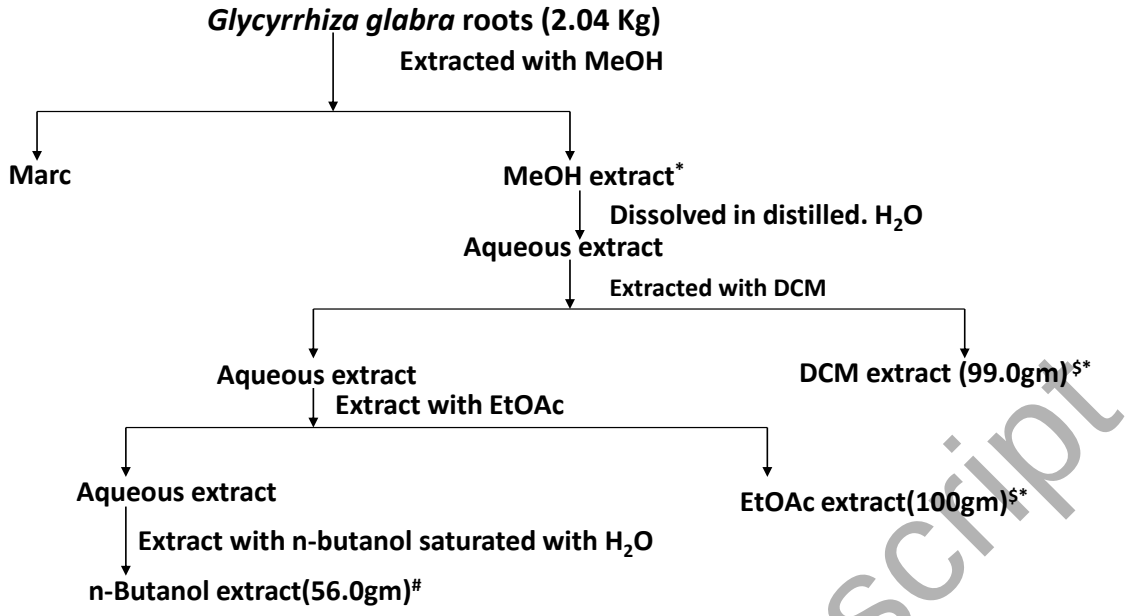

$Washed with H_2O and dried over anhydrous Na_2SO_4. *Solvent was completely removed under vacuum at 60°C on Buchi Rota Vapour. # Solvent removed under vacuum by making azeotrop with H_2O.

Figure 1: A schematic procedure for extraction and fractionation of *Glycyrrhiza glabra* roots

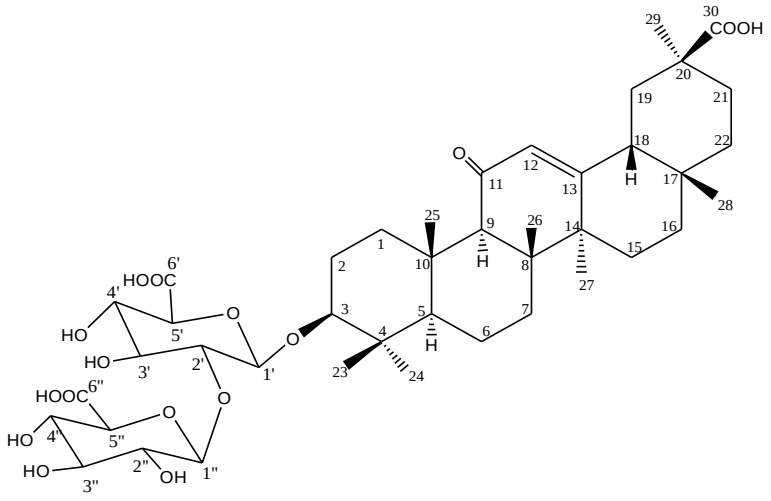

Figure **2**: Structure of glycyrrhizic acid

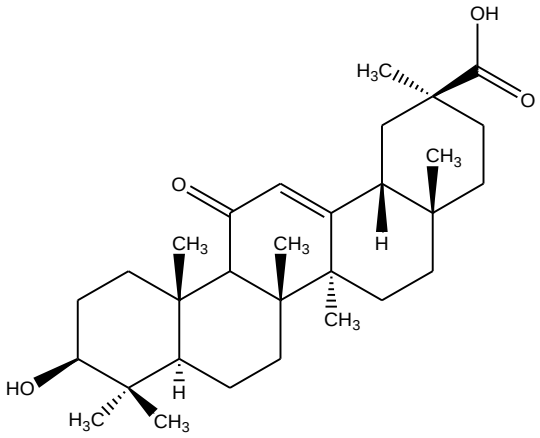

Figure **3**: Structure of glycyrrhetinic acid (GA)

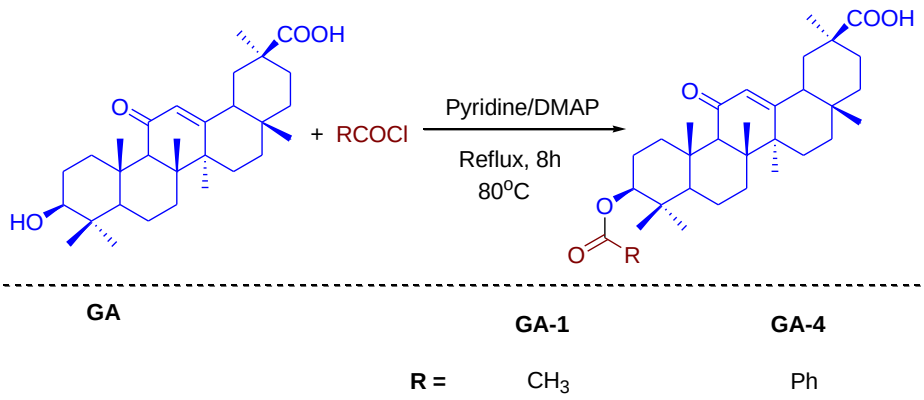

Figure **4a**: Scheme-1. Synthesis of 3-*O*-acyl derivatives of GA.

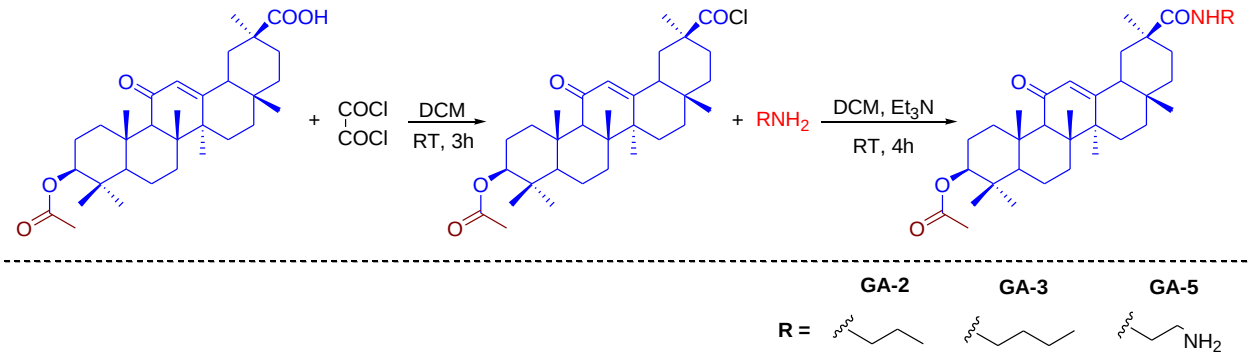

Figure **4b**: Scheme-2. Synthesis of amide derivatives of 3-*O*-acetyl GA.

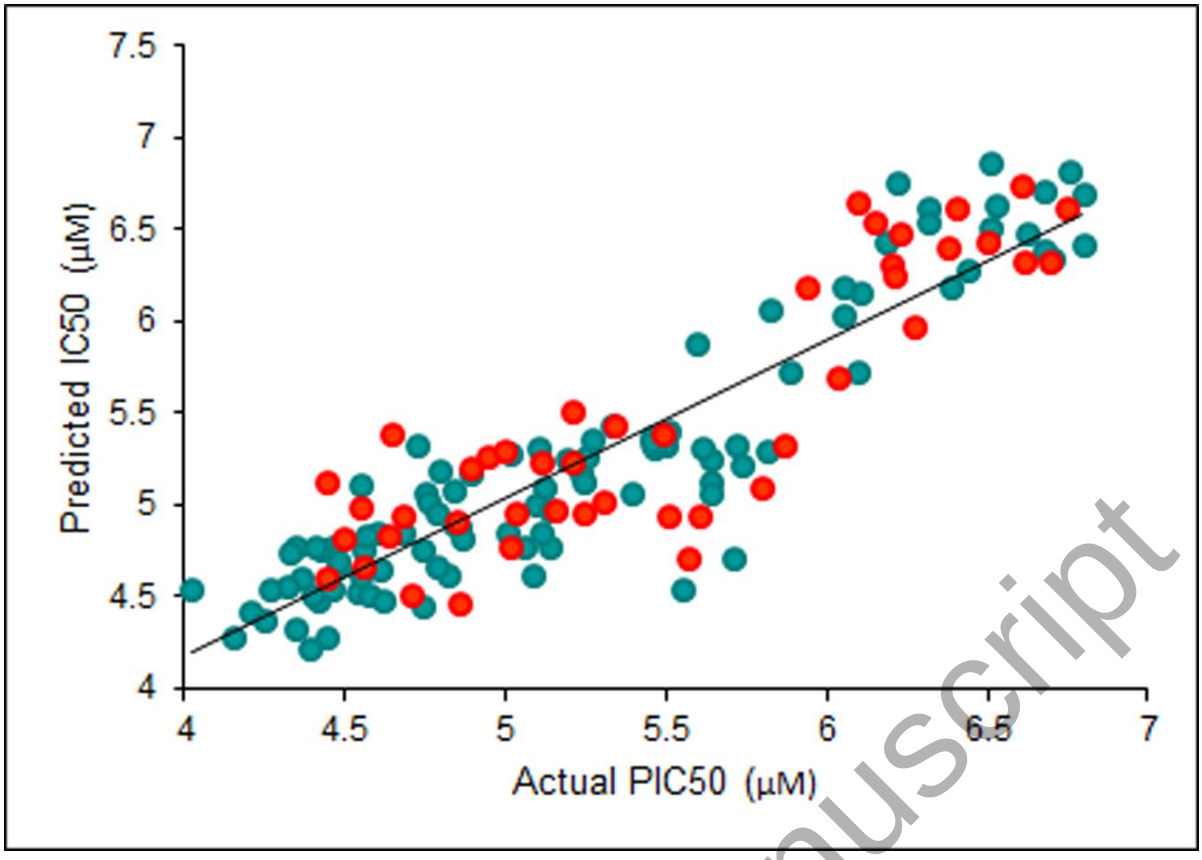

Figure **5.** Regression curve (MLR model) for actual and predicted PIC_{50} of 144 natural scaffold-based inhibitors of metastatic TNBC cell line MDA-MB-231. Training and test set compounds are highlighted with blue and red dots respectively.

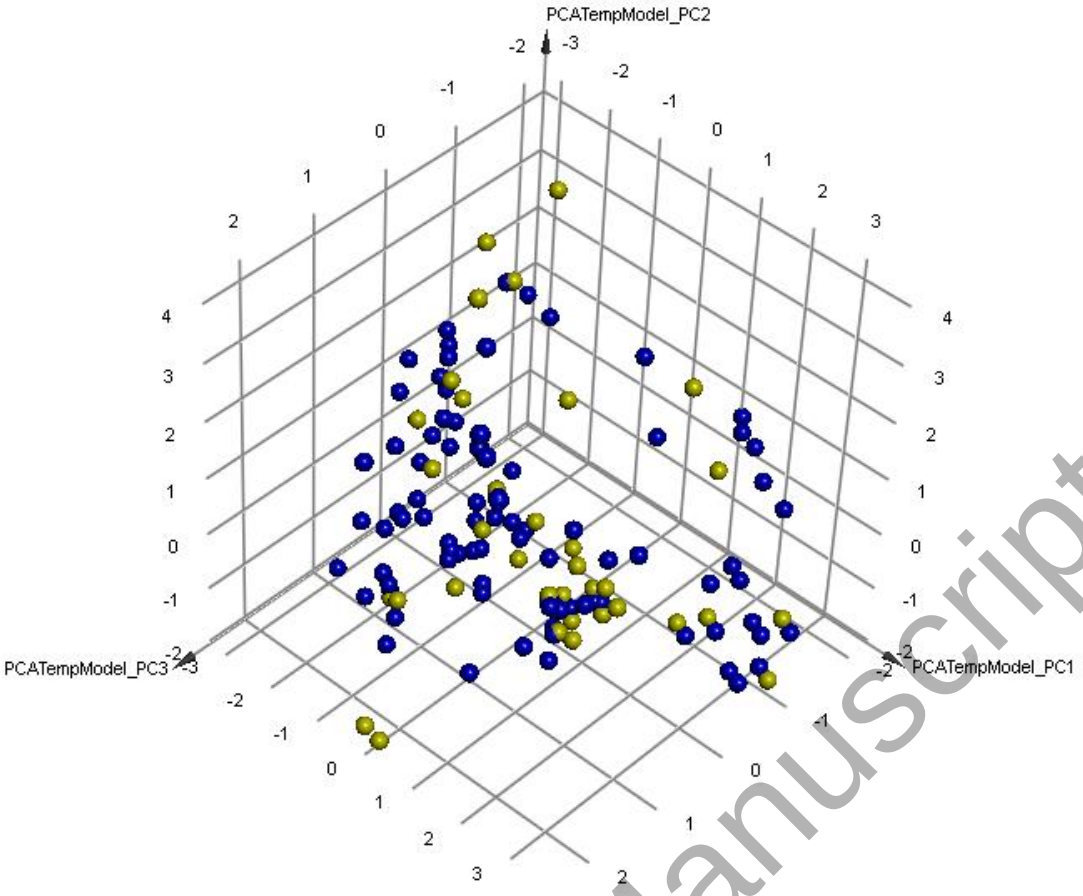

Figure 6: Generated 3D Principal Component Analysis (PCA) to ascertain uniform distribution of test set (yellow sphere) within property vector space of training set (blue sphere).

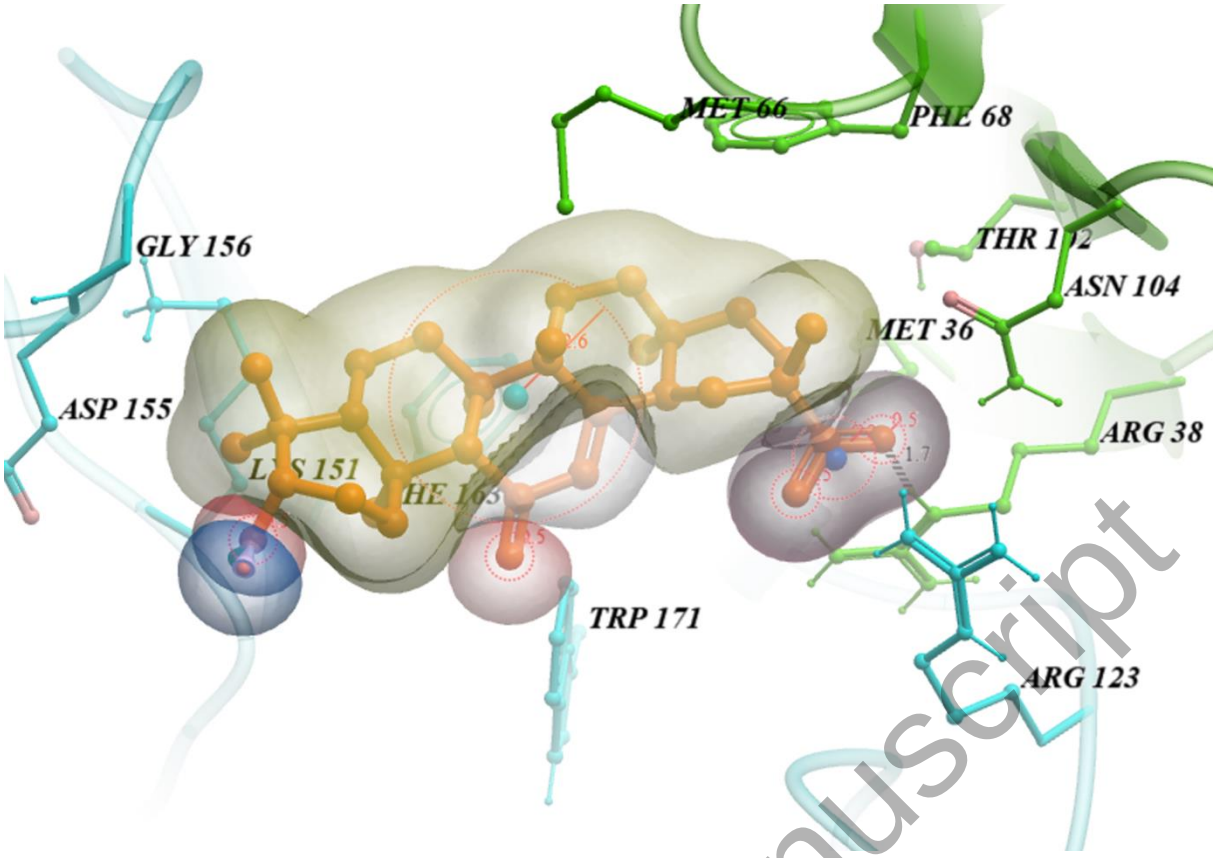

Figure **7.** The zoom in view of Glyoxalase-I bound glycyrrhetinic acid atomic property fields represented with CPK form. The white blob represented equipotential contour of lipophilic property. Red and blue blobs on carbon-3 (C-3) and carbon-30 (C-30) represented equipotential contour of hydrogen bond acceptor and donor respectively.

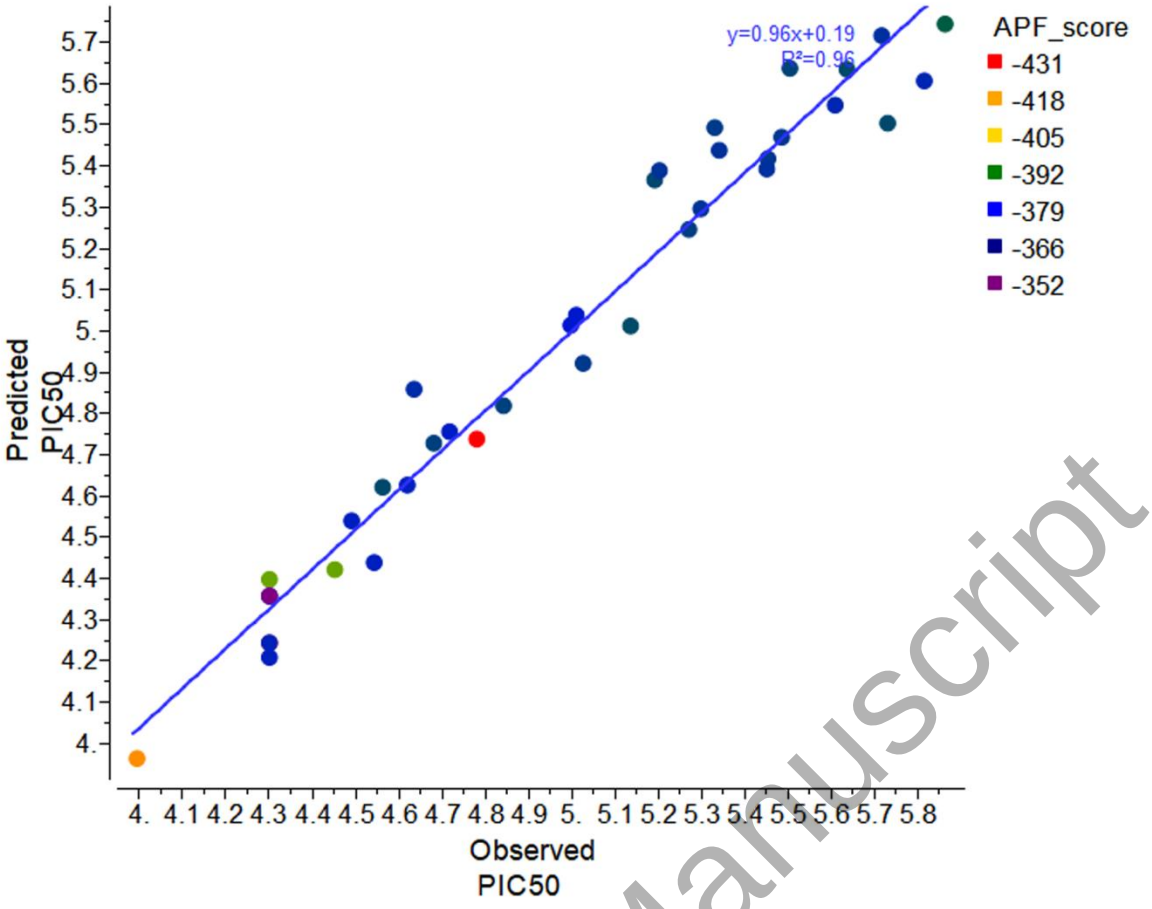

Figure 8. Regression plot for training set compounds for 3D QSAR model. Different compounds were highlighted with different color code based on APF score of training set compounds.

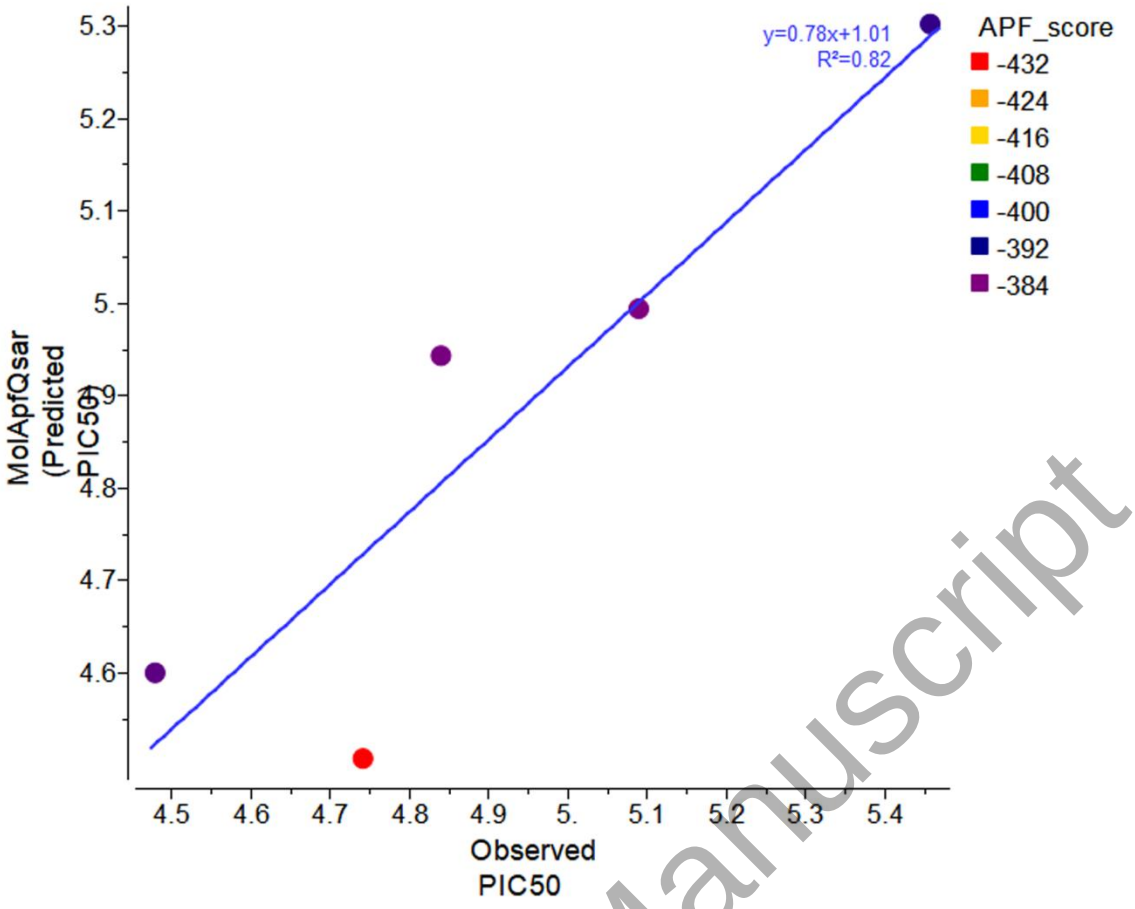

Figure **9**. Regression plot for test set compounds for 3D QSAR model. Different compounds were highlighted with different color code based on their APF score.

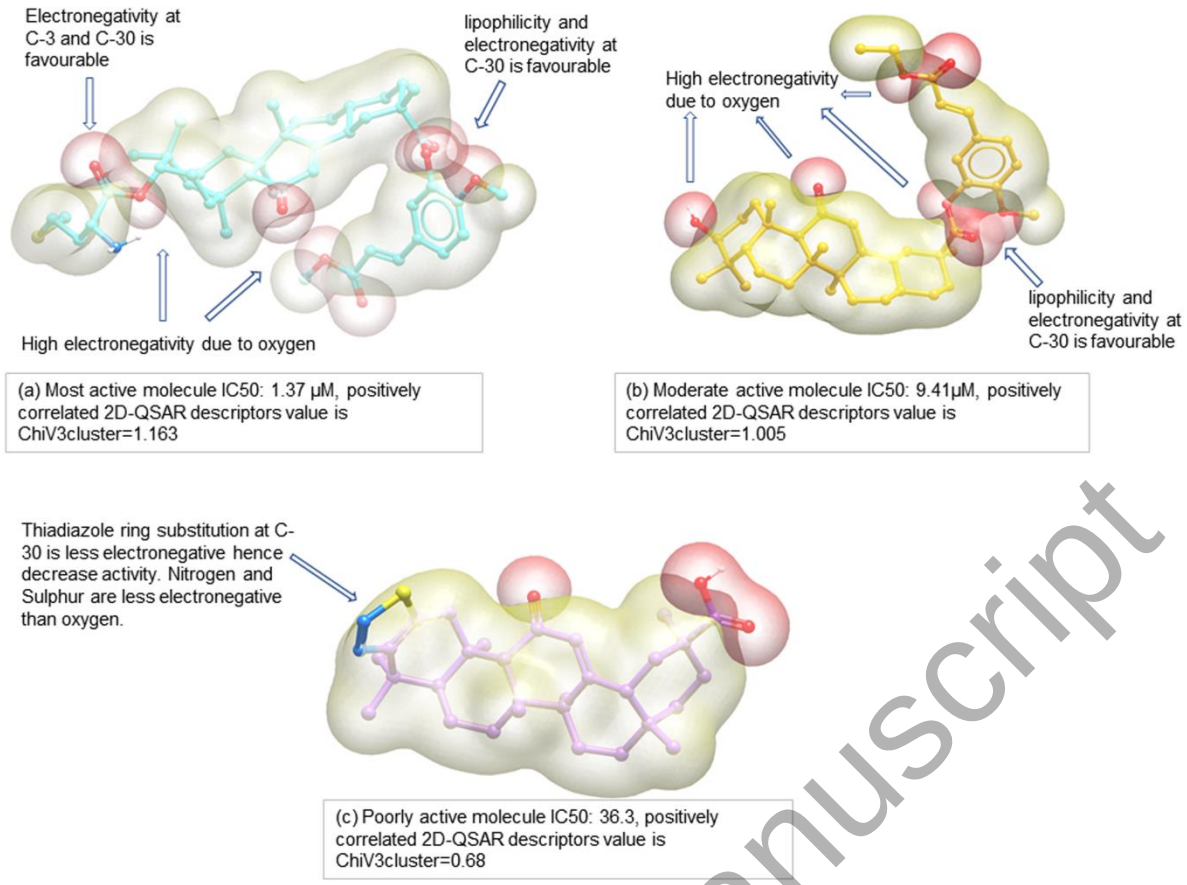

Figure 10: The APFs map of equipotent contour of most active, moderately active and least active GA derivatives used in 2D and 3D-QSAR modelling. (a) Most active GA derivative with IC_{50}: 1.37 µM, showing modification at C-3 and C-30 carbon with lipophilic branches. The most active GA derivative exhibit high 2D-QSAR descriptor Chiv3cluster value; 1.163 (b) moderately active GA derivative with IC_{50}: 9.41 µM, showing modification at C-30 carbon with lipophilic fragment. The molecule exhibits moderate Chiv3cluster value; 1.005 (c) least active GA derivative with IC_{50}: 50 µM, showing modification of C-3 carbon with 1,2,3 thiadiazol group decreases the overall activity of molecule. Least active derivative showed low 2D-QSAR descriptor Chiv3cluster value 0.68. The white blob represented equipotential contour of lipophilic property. Red blob represented equipotential contour of hydrogen bond acceptor.

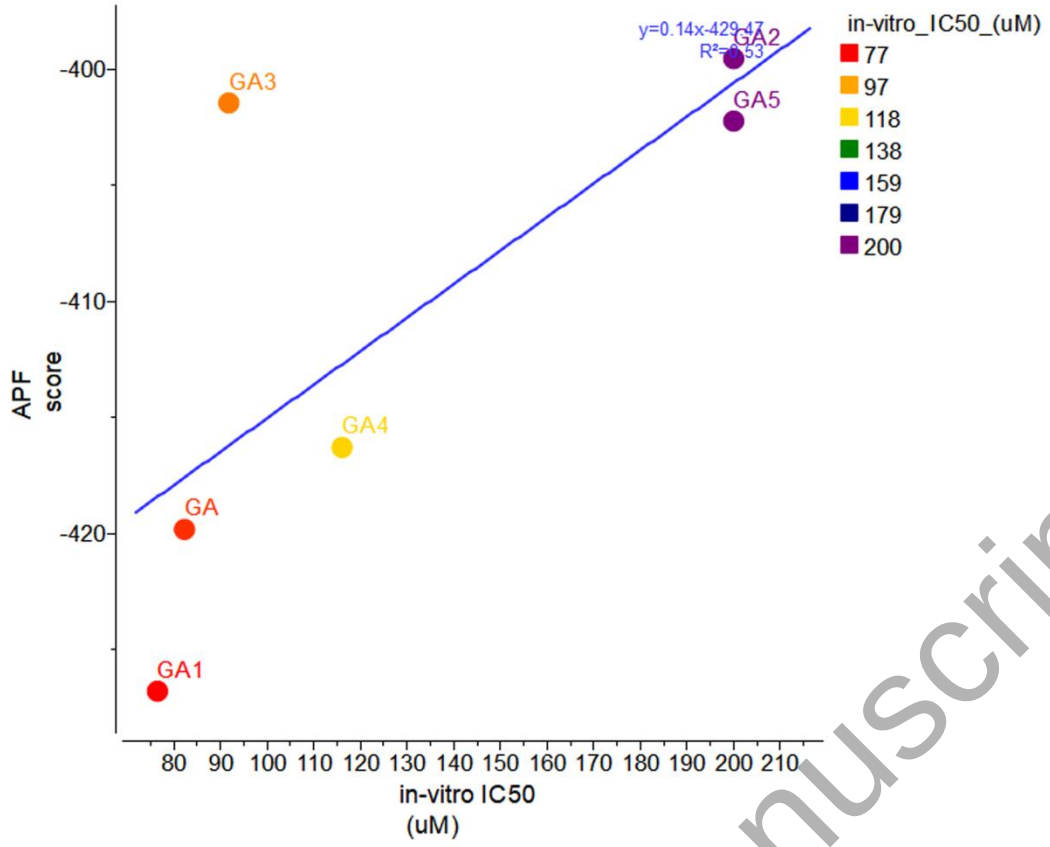

Figure 11: Figure represent a plot between *in-vitro* activity and APF scores of GA derivatives, GA-1, GA-2, GA-3, GA-4 and GA-5. The figure illustrates there is a positive correlation between atomic property fields and breast cancer inhibition of GA derivatives.

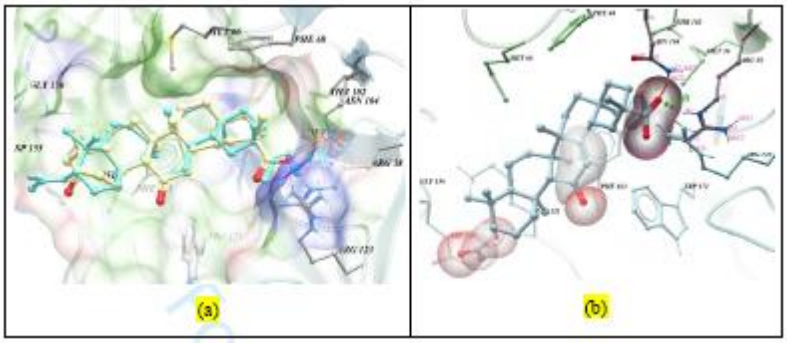

Figure **12**: Atomic property field based docking model of derivative GA-1 (cyan color ball and stick form, IC_{50}= 76.5 μM) bound to Glyoxalase-I GSH binding site. (a) The superimposition between glycyrrhetinic acid (white ball and stick form, oxygen atoms highlighted with red) and GA-1 illustrate, the GA-1 exhibit similar binding conformation as that of co-crystallised glycyrrhetinic acid. (b) A close view of GA-1 and key amino acid residue binding. Orange and green balls lines represent hydrogen bonds with GA-1 C-30 negatively charged oxygen atom (-$RCOO^-$) with polar hydrogens of amino acid residues ARG-38 (1.8 Å) and ASN-104 (2.3 Å).

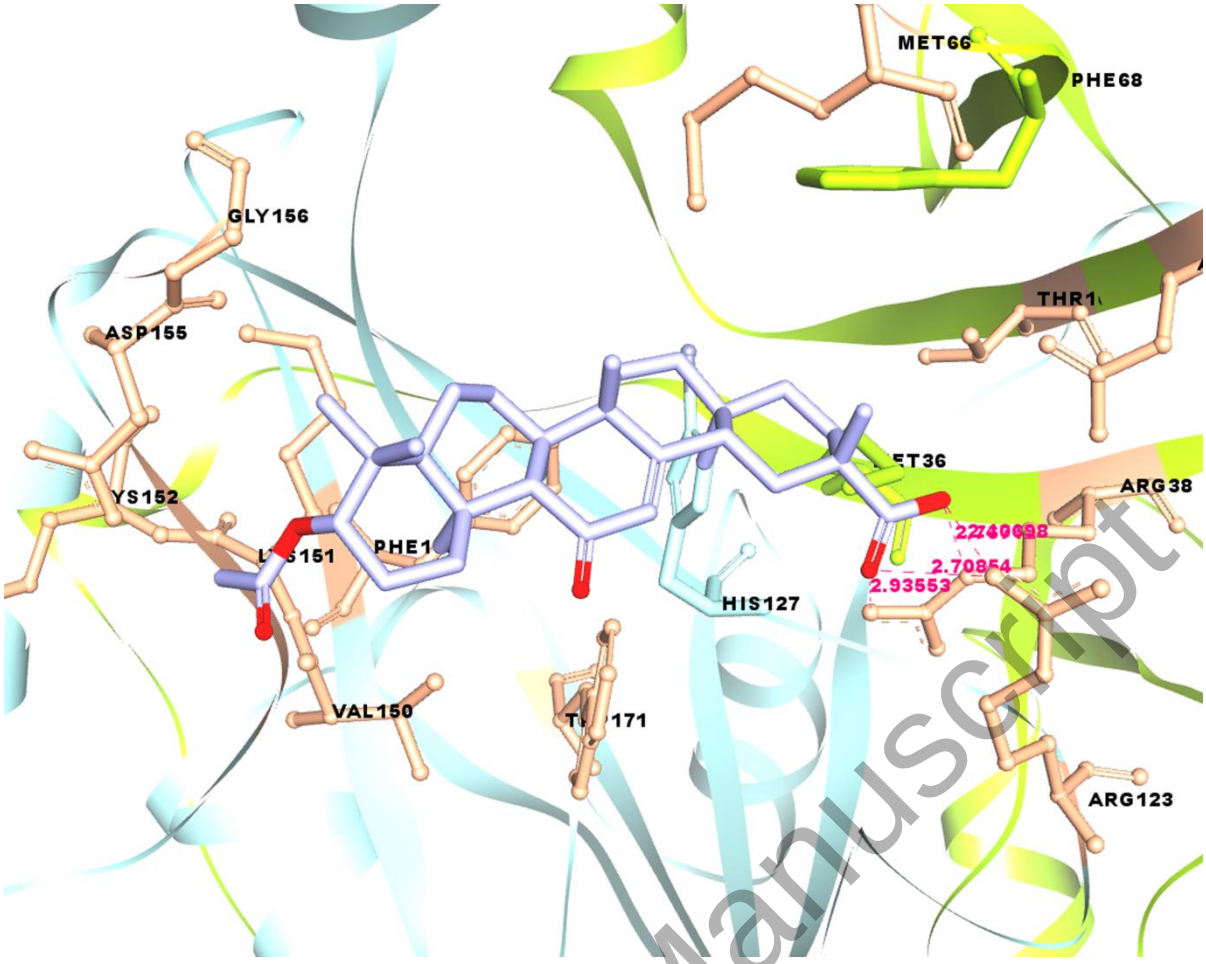

Figure **13**. Proposed binding pose of derivatives GA-1 (with binding energy-16.997 kJ/mol) on GSH binding site of Glyoxalase-I. C-30 carboxylic group of GA-1 making two hydrogen bonds with key amino acids ARG-38 and ARG-123.

Table 1: The statistical parameters and their calculated values for training set of QSAR model.

S.No.	Statistical qualities (training set)	Parameter explanation	Value	Reported acceptable range
1.	N	Training set, 70% whole dataset	100	
2.	r^2	Regression coefficient for training set	0.8442	> 0.6 (Golbraikh *et. al.,* 2002)
3.	q^2	Regression coefficient for leave one out (LOO) validation	0.8282	> 0.5 (Golbraikh *et. al.,* 2002)
4.	F-test	Fisher test	101.656	High value is good
5.	Z score for r^2	Randomization test for r^2	14.767	>1.28 at SD 0.10, (Zheng *et. al.,* 2000)
6.	Z score for q^2	Randomization test for q^2	14.617	>1.28 at SD 0.10, (Zheng *et. al.,* 2000)
7.	r_0^2	Correlation regression without intercept	0.8439	
8.	$r_0'^2$	Reciprocal of r^2_0 i.e., taking predicted value in x-axis while calculation	0.8219	
9.	r_m^2	Correlation between actual and predicted values with intercept and without intercept while calculation	0.8301	>0.5 (Ojha et. al., 2011)
10.	$r_m'^2$	Reciprocal of r^2_m i.e., taking predicted value in x-axis	0.7181	>0.5 (Ojha et. al., 2011)
11.	$\overline{r_m^2}$	Average of r^2_m and r'^2_m	0.7741	>0.5 (Ojha et. al., 2011)
12.	Δr_m^2	Absolute difference between r^2_m and r'^2_m	0.1119	<0.2 (Ojha et. al., 2011)

Table 2: The statistical parameters and their calculated values for test set of QSAR model.

S.No.	Statistical qualities (test set)	Parameter explanation	Value	Reported acceptable range
1.	n	test set, 30% of whole dataset	44	
2.	r^2_{pred}	regression coefficient for test set	0.7532	> 0.5 (Golbraikh *et. al.*, 2002)
3.	Z sore for r^2_{pred}	Randomization test for r^2_{pred}	4.11170	>1.28 at SD 0.10, (Zheng *et. al.*, 2000)
4.	r_0^2	Correlation regression without intercept	0.7410	
5.	$r_0^{/2}$	Reciprocal of r^2_0 i.e., taking predicted value in x-axis while calculation	0.7299	
6.	r_m^2	Correlation between actual and predicted values with intercept and without intercept while calculation	0.6702	>0.5 (Ojha et. al., 2011)
7.	$r_m^{/2}$	Reciprocal of r^2_m i.e., taking predicted value in x-axis	0.6384	>0.5 (Ojha et. al., 2011)
8.	$\overline{r_m^2}$	average of r^2_m and $r^{/2}_m$	0.6543	>0.5 (Ojha et. al., 2011)
9.	Δr_m^2	absolute difference between r^2_m and $r^{/2}_m$	0.0317	<0.2 (Ojha et. al., 2011)

Table 3: The statistical parameters and their calculated values for training set of APF 3D-QSAR model.

S.No.	Statistical qualities (training set)	Parameter explanation	Value	Reported acceptable range
1.	N	Training set	37	
2.	SelfMAE	Mean absolute error	0.0771089	
3.	Test_r^2	Regression coefficient for training set	0.963138	> 0.6 (Golbraikh *et. al.*, 2002)
4.	selfRMSE	Root mean square error	0.0999803	
5.	SelfMAE	Mean absolute error	0.0771089	
6.	Self-spearman	Spearman regression coefficient	0.98056	
7.	r_0^2	Correlation regression without intercept	0.9632	
8.	$r_0'^2$	Reciprocal of r^2_0 i.e., taking predicted value in x-axis while calculation	0.9617	
9.	r_m^2	Correlation between actual and predicted values with intercept and without intercept while calculation	0.90555	>0.5 (Ojha et. al., 2011)
10.	$r_m'^2$	Reciprocal of r^2_m i.e., taking predicted value in x-axis	0.9203	>0.5 (Ojha et. al., 2011)
11.	$\overline{r_m^2}$	Average of r^2_m and r'^2_m	0.9129	>0.5 (Ojha et. al., 2011)
12.	Δr_m^2	Absolute difference between r^2_m and r'^2_m	-0.0147	<0.2 (Ojha et. al., 2011)

Table 4: The statistical parameters and their calculated values for test set of APF 3D-QSAR model.

S.No.	Statistical qualities (test set)	Parameter explanation	Value	Reported acceptable range
1.	n	test set	5	
2.	SelfMAE	Mean absolute error	0.2772	
3.	r^2	regression coefficient for test set	0.82	> 0.5 (Golbraikh *et. al.*, 2002)
4.	$testr^2(LOO)$	Regression coefficient for test set leave one out (LOO) validation	0.6502	> 0.6 (Golbraikh *et. al.*, 2002)
5.	testRMSE	Root mean square error	0.3279	
6.	Test Spearman	Spearman regression coefficient	0.8207	
7.	r_0^2	Correlation regression without intercept	0.8196	
8.	$r_0'^2$	Reciprocal of r^2_0 i.e., taking predicted value in x-axis while calculation	0.7659	
9.	r_m^2	Correlation between actual and predicted values with intercept and without intercept while calculation	0.8043	>0.5 (Ojha et. al., 2011)
10.	$r_m'^2$	Reciprocal of r^2_m i.e., taking predicted value in x-axis	0.6269	>0.5 (Ojha et. al., 2011)
11.	$\overline{r_m^2}$	Average of r^2_m and r'^2_m	0.7157	>0.5 (Ojha et. al., 2011)
12.	Δr_m^2	Absolute difference between r^2_m and r'^2_m	0.17737	<0.2 (Ojha et. al., 2011)

Table **5**: SRB based *in-vitro* cytotoxic activity of GA, GA-1, GA-2, GA-3, GA-4 and GA-5 against metastatic triple negative breast cancer cell line MDA-MB-231.

Compounds	*In-vitro* IC_{50} (µM)
Glycyrrhetinic acid	82.29
GA-1	76.5
GA-2	>200
GA-3	91.79
GA-4	116.07
GA-5	>200

Table **6**: Compliance of atomic property filed score and FlexX binding energy of Glycyrrhetinic acid, GA-1, GA-2, GA-3, GA-4 and GA-5 on Glyoxalase-I GSH binding site.

Compounds	APF* score	FlexX binding energy kJ/mol
Glycyrrhetinic acid (positive control)	-419.617182	-25.561
GA-1	-425.82269	-16.997
GA-2	-402.04735	-9.7
GA-3	-401.184344	-7.293
GA-4	-415.679134	-21.232
GA-5	-402.136577	-10.419